ornl

NUREG/CR-3830
Volume 1
ORNL/TM-9217/V1

OAK RIDGE
NATIONAL
LABORATORY

MARTIN MARIETTA

Aerosol Release and Transport Program Semiannual Progress Report for October 1983–March 1984

R. E. Adams M. L. Tobias

Prepared for the U.S. Nuclear Regulatory Commission
Office of Nuclear Regulatory Research
Under Interagency Agreements DOE 40-551-75 and 40-552-75

OPERATED BY
MARTIN MARIETTA ENERGY SYSTEMS, INC.
FOR THE UNITED STATES
DEPARTMENT OF ENERGY

Printed in the United States of America. Available from
National Technical Information Service
U.S. Department of Commerce
5285 Port Royal Road, Springfield, Virginia 22161

Available from

GPO Sales Program
Division of Technical Information and Document Control
U.S. Nuclear Regulatory Commission
Washington, D.C. 20555

NUREG/CR-3830
Volume 1
ORNL/TM-9217/V1
Dist. Category R7

Engineering Technology Division

AEROSOL RELEASE AND TRANSPORT PROGRAM SEMIANNUAL PROGRESS REPORT FOR OCTOBER 1983–MARCH 1984

R. E. Adams M. L. Tobias

Manuscript Completed – June 29, 1984
Date Published – August 1984

Prepared for the
U.S. Nuclear Regulatory Commission
Office of Nuclear Regulatory Research
Under Interagency Agreements DOE 40-551-75 and 40-552-75

NRC FIN No. B0121
NRC FIN No. B0476

Prepared by the
OAK RIDGE NATIONAL LABORATORY
Oak Ridge, Tennessee 37831
operated by
MARTIN MARIETTA ENERGY SYSTEMS, INC.
for the
U.S. DEPARTMENT OF ENERGY
under Contract No. DE-AC05-840R21400

CONTENTS

	Page
LIST OF FIGURES	v
LIST OF TABLES	vii
FOREWORD	ix
SUMMARY	xi
GLOSSARY OF ACRONYMS	xiii
ABSTRACT	1
1. INTRODUCTION	1
2. EXPERIMENTAL PROGRAM	3
2.1 Source-Term Experiments in FAST/CRI-III	3
2.1.1 Introduction	3
2.1.2 Discussion of FAST undersodium test results	9
2.2 Secondary Containment Aerosol Studies in the NSPP	23
2.2.1 Introduction	23
2.2.2 LWR aerosol experiment 613	23
2.2.3 LWR aerosol experiment 631	26
2.2.4 Influence of steam environment on behavior of mixed Fe_2O_3 + U_3O_8 aerosol	31
2.3 Basic Aerosol Experiments	31
2.4 Core-Melt ART Project	35
2.4.1 Introduction	35
2.4.2 LWR core-melt release correlation with MARCH accident sequences	36
2.4.3 Release rates calculated from accumulated release totals	39
2.4.4 Volatility of boric oxide in a core-melt environment	41
2.4.5 Initial operation of the new 250-kW induction generator	43
2.4.6 Fuel and control rod procurement	44
2.4.7 Program plan	52
3. ANALYTICAL PROGRAM	53
3.1 Introduction	53
3.2 Comparison of NAUA Code Predictions with NSPP Aerosol Experiments in Steam-Air Atmospheres	53
3.2.1 Effect of diffusional boundary layer thickness	54
3.2.2 Effect of assumed initial particle size	56

3.2.3 Effect of assumed source rate at an assumed initial radius of 1 μm 56
3.2.4 Diffusiophoretic effects 57
3.2.5 Numerical effects 59
3.2.6 Conclusions 60
3.3 FAST-Related Code Development Work 60
REFERENCES 62

LIST OF FIGURES

Figure		Page
1	Schedule for FAST/CRI-III tests	4
2	Schematic of FAST test vessel	5
3	Schematic of test sample in underwater and under-sodium tests	5
4	Comparison of oscilloscope pressure traces in (a) FAST-105, (b) FAST-107, and (c) FAST-108	10
5	Expanded views of oscilloscope sodium pressure traces in (a) FAST-105, (b) FAST-107, and (c) FAST-108	11
6	Expanded views of oscilloscope cover-gas pressure traces in (a) FAST-105, (b) FAST-107, and (c) FAST-108	12
7	Expanded views of oscilloscope sodium-pressure trace in (a) FAST-112, (b) FAST-110, and (c) FAST-109	14
8	Expanded views of oscilloscope cover-gas pressure traces in (a) FAST-112, (b) FAST-110, and (c) FAST-109	15
9	Aerosol sampling results for FAST sodium tests conducted at argon cover-gas pressure of 120 kPa (abs) and xenon fuel sample pressure of 340 kPa (abs)	22
10	Aerosol sampling results for FAST sodium tests conducted at argon cover-gas pressure of 300 kPa (abs) and xenon fuel sample pressure of 340 kPa (abs)	23
11	Aerosol concentration (Fe_2O_3) as function of time in steam environment (NSPP No. 613)	25
12	Average aerosol mass concentrations as function of time for Fe_2O_3 and U_3O_8 components of mixed aerosol in a steam environment (NSPP No. 613)	27
13	Aerosol concentration (U_3O_8) as function of time in dry air (RH < 20%) environment (NSPP No. 631)	28
14	Average aerosol mass concentrations as function of time for Fe_2O_3 and U_3O_8 components of mixed aerosol in dry air (RH < 20%) environment (NSPP No. 613)	30
15	Comparison of behavior of mixed aerosols (Fe_2O_3 + U_3O_8) in steam-air environment (NSPP Nos. 611–613)	33
16	Comparison of behavior of mixed aerosols (Fe_2O_3 + U_3O_8) in steam-air and dry air environments	34

17	Reactor accident Surry ABγ-2 sequence	37
18	Accumulated release fraction (R_{cm}) for core-melt	40
19	Rate of aerosol release for AB sequence	41
20	Housing and furnace for 10-kg fuel melting system	45
21	Design of large induction furnace with elevating jack	46
22	Comparative sizes of 1-kg and 10-kg fuel bundles	47
23	The 10-kg core-melt components and 62-rod fuel bundle	48
24	New 250-kW induction generator of ORNL	49
25	Induction generator and transmission and cooling system	50
26	Initial test of mock-up bundle at elevated temperature	51
27	Experiment 501, iron oxide in steam	54
28	Comparison of HAARM-3 calculations with iron oxide—steam experiment 504	55
29	Experiment 504, iron oxide in steam	56
30	Experiment 504, iron oxide in steam	57
31	Experiment 401, uranium oxide in steam	58
32	Experiment 501, iron oxide in steam	58
33	Experiment 504, iron oxide in steam	59
34	Experiment 504	60

LIST OF TABLES

Table		Page
1	FAST single-pin undersodium test plan	6
2	Test specimen data	6
3	Test conditions	7
4	Electrical energy input data	8
5	Sodium pressure maximum and minimum points in FAST-108	13
6	Sodium pressure maximum and minimum points from FAST-112, FAST-110, and FAST-109	16
7	Aerosol sampling results for FAST-104	17
8	Aerosol sampling results for FAST-105	17
9	Aerosol sampling results for FAST-106	18
10	Aerosol sampling results for FAST-107	18
11	Aerosol sampling results for FAST-108	19
12	Aerosol sampling results for FAST-109	19
13	Aerosol sampling results for FAST-110	20
14	Aerosol sampling results for FAST-111	20
15	Aerosol sampling results for FAST-112	21
16	Location of NSPP aerosol mass concentration samplers	24
17	Results from aerosol sizing samples (NSPP No. 631)	29
18	Summary of NSPP experimental details and results	32
19	Accumulated release fractions for ABγ-2	38
20	Values for the constants in Eq. (2)	40
21	Aerosol release rate for core-melt ABγ-2 accident sequence	42
22	Summary of boron release experiments	43
23	Results of experiment CM-40 on the volatility of boric acid added as emergency control coolant	44
24	NSPP steam-uranium oxide aerosol experiments	53
25	NSPP steam-iron oxide aerosol experiments	54

FOREWORD

This report summarizes progress under the Aerosol Release and Transport Program [sponsored by the Division of Accident Evaluation, Office of Nuclear Regulatory Research, Nuclear Regulatory Commission (NRC)] for the period October 1983–March 1984.

Work on this program was initially reported as Volume III of a four-volume series entitled *Quarterly Progress Report on Reactor Safety Programs Sponsored by the NRC Division of Reactor Safety Research*. Prior reports of this series are

Report No.	Period covered
ORNL/TM-4655	April–June 1974
ORNL/TM-4729	July–September 1974
ORNL/TM-4805	October–December 1974
ORNL/TM-4914	January–March 1975
ORNL/TM-5021	April–June 1975

Beginning with the report covering the period July–September 1975 through the report for the period July–September 1981, work under this program was reported as *LMFBR Aerosol Release and Transport Program Quarterly Progress Report*. Prior reports under this title are

Report No.	Period covered
ORNL/NUREG/TM-8	July–September 1975
ORNL/NUREG/TM-9	October–December 1975
ORNL/NUREG/TM-35	January–March 1976
ORNL/NUREG/TM-59	April–June 1976
ORNL/NUREG/TM-75	July–September 1976
ORNL/NUREG/TM-90	October–December 1976
ORNL/NUREG/TM-113	January–March 1977
ORNL/NUREG/TM-142	April–June 1977
ORNL/NUREG/TM-173	July–September 1977
ORNL/NUREG/TM-193	October–December 1977
ORNL/NUREG/TM-213	January–March 1978
ORNL/NUREG/TM-244	April–June 1978
ORNL/NUREG/TM-276	July–September 1978
ORNL/NUREG/TM-318	October–December 1978
ORNL/NUREG/TM-329	January–March 1979
ORNL/NUREG/TM-354	April–June 1979
ORNL/NUREG/TM-376	July–September 1979
ORNL/NUREG/TM-391	October–December 1979
ORNL/NUREG/TM-416	January–March 1980
ORNL/NUREG/TM-417	April–June 1980
ORNL/TM-5806	July–September 1980
ORNL/TM-7884	October–December 1980
ORNL/TM-7946	January–March 1981
ORNL/TM-7974	April–June 1981
ORNL/TM-8149	July–September 1981

Beginning with the report covering the period October–December 1981, work under the program was reported as *Aerosol Release and Transport Program Quarterly Progress Report*. Prior reports under this title are

Report No.	Period covered
ORNL/TM-8307	October–December 1981
ORNL/TM-8397/V1	January–March 1982
ORNL/TM-8397/V2	April–June 1982
ORNL/TM-8397/V3	July–September 1982
ORNL/TM-8397/V4	October–December 1982
ORNL/TM-8849/V1	January–March 1983
ORNL/TM-8849/V2	April–June 1983
ORNL/TM-8849/V3	July–September 1983

Beginning with the report covering the period October 1983–March 1984, work under the program is now being reported as *Aerosol Release and Transport Program Semiannual Progress Report*. Copies of all these reports are available from the Technical Information Center, Oak Ridge, Tennessee 37831.

SUMMARY

M. L. Tobias

The Aerosol Release and Transport (ART) Program at Oak Ridge National Laboratory (ORNL) is designed to investigate the release, transport, and behavior of aerosols that may carry radionuclides originating from a severe accident resulting in core melting. Aspects of the program apply to both light-water reactors (LWRs) and liquid-metal fast breeder reactors (LMFBRs). The experimental programs are being conducted in the Fuel Aerosol Simulant Test (FAST) Facility (which also includes the CRI-III vessel), the NSPP Facility, and the CRI-II Facility. The analytical efforts are designed to support the experiments and to provide comparisons between the experimental observations and the results of computer codes intended to simulate aerosol behavior.

During this period, two important program changes have occurred. The first was the decision to terminate the LMFBR aspects of the program carried out in the FAST Facility. Studies are under way to determine the possibilities of performing LWR-related studies in FAST and CRI-III. The second is the decision to separate the core-melt aerosol release project from the ART program in order to accommodate a change in objective and an enlargement in scope. Future activities in this project will be reported elsewhere.

In the program of experiments in the FAST/CRI-III Facilities, tests FAST-108 through FAST-112 were conducted. In FAST-108, the sodium height was 7.7 cm, argon cover-gas pressure was 120 kPa (abs), xenon pressure in the fuel assembly was 340 kPa (abs), and sodium temperature was 813 K. The energy input to the UO_2 fuel was 19.6 kJ over a period of 1.55 ms before disassembly. This test was the last in a group of four (FAST-105 through FAST-108) in which sodium height was varied. FAST-109, FAST-110, and FAST-112 were the first tests of a group at an argon pressure of 300 kPa. Sodium heights above the fuel sample were 9.5, 14, and 25 cm, respectively, and xenon pressure and sodium temperature were the same as in FAST-108.

Examination of initial bubble oscillation period for the series FAST-105 through FAST-107 showed a decrease with decrease in sodium height. In FAST-108 and FAST-109, however, bubble oscillation patterns are much less clear. Oscilloscope pressure traces of the runs at 300 kPa cover-gas pressure show much shorter bubble oscillation periods than those obtained for 120 kPa.

Aerosol sampling results for FAST-104 through FAST-112 are reported. Very strong attenuation of the aerosol by the sodium was noted in all cases; less than 10^{-3} of the fuel vapor was found in the cover gas. No increase of aerosol concentration in the cover gas with decreasing sodium level was noted. As a check, the FAST-111 test was run with the sample completely above the sodium, and the results demonstrated the adequacy of aerosol sampling methods, agreeing well with earlier argon atmosphere tests.

In the program of NSPP experiments, tests 613 and 631 were performed. Experiment 613 involved simultaneous generation of U_3O_8 and Fe_2O_3 aerosols in steam with a target ratio of 10 to 1 (Fe_2O_3 to U_3O_8). The vessel atmosphere was at 0.178 MPa (abs) and 381 K during aerosol injection, rising to 0.220 MPa and 386 K in the subsequent 6 h of steam injection. The ratio actually achieved was 9.6 to 1, corresponding to concentrations of 6.8 and 0.71 $\mu g/cm^3$ for Fe_2O_3 and U_3O_8, respectively. In test 631, the U_3O_8 and Fe_2O_3 mixture was generated in a dry environment (relative humidity less than 20%) at ambient pressure and temperature. The U_3O_8 to Fe_2O_3 mass ratio achieved was about 1.2 to 1. The aerosol appeared to remain airborne longer than aerosol mixtures generated in steam atmosphere. The aerosol was in the form of chain agglomerates rather than spherical clumps, and coagglomeration appears to have occurred.

Support work for the DEMONA (West Germany) and Marviken (Sweden) projects continues. Primary efforts during this period have been in the area of aerosol generator development. A small Lovelace Aerosol Particle Separator is being refitted to adapt it to the 250-V 50-cycle Swedish electrical power system. In addition, a variable-speed option will be provided to improve the size discrimination range for larger particles.

In the program of LWR core-melt studies, final results of test CM-37 show that only 1.03% of the boron carbide escaped as boric oxide from the melt under the hydrolysis-oxidation conditions of this experiment. In experiment CM-38, the relative volatility of B_2O_3 when mixed with UO_2 was studied. The boron release was only about one-half that in CM-37. In a similar experiment, CM-39, the boric oxide was mixed with powdered ZrO_2, and about 0.9% of the boric oxide was released. The final boric oxide test was CM-40, in which the boric oxide was added to the feedwater used to generate steam in the experiment. About 10% of the boron was vaporized as oxide during the lower temperature heating steps, but as temperature was increased, the release appeared to have stopped.

The 250-kW radio-frequency induction furnace was successfully operated in a test in which a simulated large fuel bundle was heated almost to the melting point (~1450°C). At full power, this took 30 s; at one-half power, about 45 s was needed. Modifications in the power supply systems have been made to increase heating efficiency.

In NSPP-related analytical program work, results from the NAUA code were compared with various NSPP experiments involving steam and iron oxide or uranium oxide aerosols. Effects of assumed diffusional boundary layer thickness, initial particle size, source rate, diffusiophoresis, and numerical procedures are discussed.

In analytical work connected with the FAST program, work continued on improvements in the UVABUBL-II code. Changes were made to account for xenon gas content in the fuel sample more accurately. Differences in results obtained on the University of Virginia's computer and the IBM-3033 at ORNL have been noted and the causes are being investigated.

GLOSSARY OF ACRONYMS

ABCOVE	Aerosol Behavior Code Validation and Evaluation
AMMD	aerodynamic mass median diameter
ART	aerosol release and transport
ATT	Aerosol Transport Test
BCL	Battelle-Columbus Laboratories
CDA	core-disruptive accident
CDV	capacitor discharge vaporization
CRBR	Clinch River Breeder Reactor
CRI-II	name of a facility for conducting basic aerosol experiments (originally, Containment Research Installation)
CSTF	Containment Systems Test Facility
DEMONA	name of an aerosol experimental facility at Battelle-Frankfurt (Demonstration Nuklearen Aerosolverhaltens)
FAST	Fuel Aerosol Simulant Test
GSD	geometric standard deviation
HCDA	hypothetical core-disruptive accident
ICP	inductively coupled plasma (spectrometric method)
ITRI	Inhalation Toxicology Research Institute
KfK	Kernforschungszentrum Karlsruhe
LANL	Los Alamos National Laboratory
LMFBR	liquid-metal fast breeder reactor
LWR	light-water reactor
NRC	Nuclear Regulatory Commission
NSPP	name of a facility in which secondary containment aerosol experiments are conducted (originally, Nuclear Safety Pilot Plant)
ORNL	Oak Ridge National Laboratory
PSL	polystyrene latex
PT	plasma torch
PWR	pressurized-water reactor
rf	radio frequency
SASCHA	name of a core-melt experiment facility at KfK (Schmelzanlage fuer Proben mit Schwacher Aktivitaet)
WROS	wall run-off sampler

AEROSOL RELEASE AND TRANSPORT PROGRAM SEMIANNUAL PROGRESS REPORT FOR OCTOBER 1983—MARCH 1984

R. E. Adams M. L. Tobias

ABSTRACT

This report summarizes progress for the Aerosol Release and Transport Program sponsored by the Nuclear Regulatory Commission, Office of Nuclear Regulatory Research, Division of Accident Evaluation, for the period October 1983—March 1984. Topics discussed include (1) the experimental program in the Fuel Aerosol Simulant Test (FAST) Facility, (2) NSPP experiments involving mixtures of aerosols of iron oxide and uranium oxide in steam and dry atmospheres, (3) support work for the DEMONA (West Germany) and Marviken (Sweden) projects, (4) analysis of core-melt experiments involving boric oxide volatility, (5) initial operation of the new 250-kW induction generator, (6) comparisons of NAUA results with experiments, and (7) tests and improvements in the UVABUBL-II code.

---

1. INTRODUCTION

The Aerosol Release and Transport (ART) Program at Oak Ridge National Laboratory (ORNL), sponsored by the Nuclear Regulatory Commission, Office of Nuclear Regulatory Research, Division of Accident Evaluation, is a safety program concerned with aerosol release and transport. The program scope includes aerosol release from fuel, transport to and release from primary containment boundaries, and behavior within containments. The overall goal of the program is to provide the analytical methods and experimental data necessary to assess the quantity and transient behavior of radioactive aerosols released from reactor cores as a result of postulated events of varying severity up to and including accidents resulting in core melting.

The program is divided into several related experimental and analytical activities:

1. development of apparatus to investigate the characteristics and transport behavior of materials vaporized from molten fuel;
2. study of the characteristics and behavior of fuel-simulant aerosols in several small vessels;
3. production and study of aerosols in the NSPP for the validation of models, with particular emphasis on the behavior of mixtures of nuclear aerosol species relevant to light-water reactor (LWR) systems.
4. studies related to liquid-metal fast breeder reactor hypothetical core-disruptive accidents (HCDAs) that involve fuel interactions,

expansion, and thermal behavior within the sodium pool as the resultant fuel vapor bubble is produced and transported through the sodium to the cover-gas region.

5. comparison of the results of experiments with calculations using existing aerosol computer codes or with specifically developed analytical procedures.

2. EXPERIMENTAL PROGRAM

2.1 Source-Term Experiments in FAST/CRI-III (B0476)

A. W. Longest
J. C. Petrykowski
W. A Bird*
J. M. Rochelle†
C. V. Hardin

2.1.1 Introduction

The Fuel Aerosol Simulant Tests (FAST) and the Containment Research Installation-III (CRI-III) tests are performed by using the capacitor discharge vaporization (CDV) technique to place UO_2 fuel samples into the high-energy states that could be produced in LMFBR HCDAs. The primary goal of the FAST/CRI-III test program is to use the experimental results as a data base for developing analytical models that could be used to predict fuel transport through the coolant in severe accidents.

During this report period, the fifth through the ninth tests (FAST-108 through FAST-112) of a planned series of ten undersodium UO_2 fuel vaporization experiments were performed in accordance with the test schedule and test plan shown in Fig. 1 and Table 1, respectively. These experiments are designed to study fuel bubble behavior and fuel aerosol transport to the cover gas as a function of sodium height above the fuel sample assembly, cover-gas pressure, and xenon gas pressure in the fuel sample assembly (to simulate fission gas in reactor fuel). FAST-108 was the last of a subset of four experiments in which the sodium height above the fuel assembly was varied while holding the argon cover gas and xenon pressures constant; FAST-109, FAST-110, and FAST-112 were the first three tests of a second similar subset at a higher cover-gas pressure (see Table 1). The FAST-111 test represents a revision in the original test plan;[1] it was conducted to determine aerosol behavior over sodium at 540°C and to verify the aerosol sampling techniques being used. Pressure measurements were made in the sodium at a distance of 23 cm from the test sample and in the cover gas above the sodium. Aerosol samples were obtained from the cover-gas region in each test. A schematic of the FAST test vessel showing the locations of the two pressure transducers, the eight-stage mass sampler used in obtaining the aerosol samples, and other equipment is given in Fig. 2. Details of the test sample assembly (vaporizer unit in Fig. 2) are shown in Fig. 3.

Test specimen data, test conditions, and electrical input data for all the tests conducted to date are presented in Tables 2–4 for convenient reference. Also included for comparison are data from FAST-103, the last test that was conducted prior to a 1-year shutdown of the facilities.[2] Only one other undersodium fuel vaporization test (FAST-101 at a much lower high-preheat level of 1100 W) and one undersodium preheat-only test (FAST-102) were performed previously.[3] The preheat stage of the two-stage electrical process for the fuel vaporization is designed to

---

*Instrumentation and Controls Division.

†Consultant from University of Tennessee.

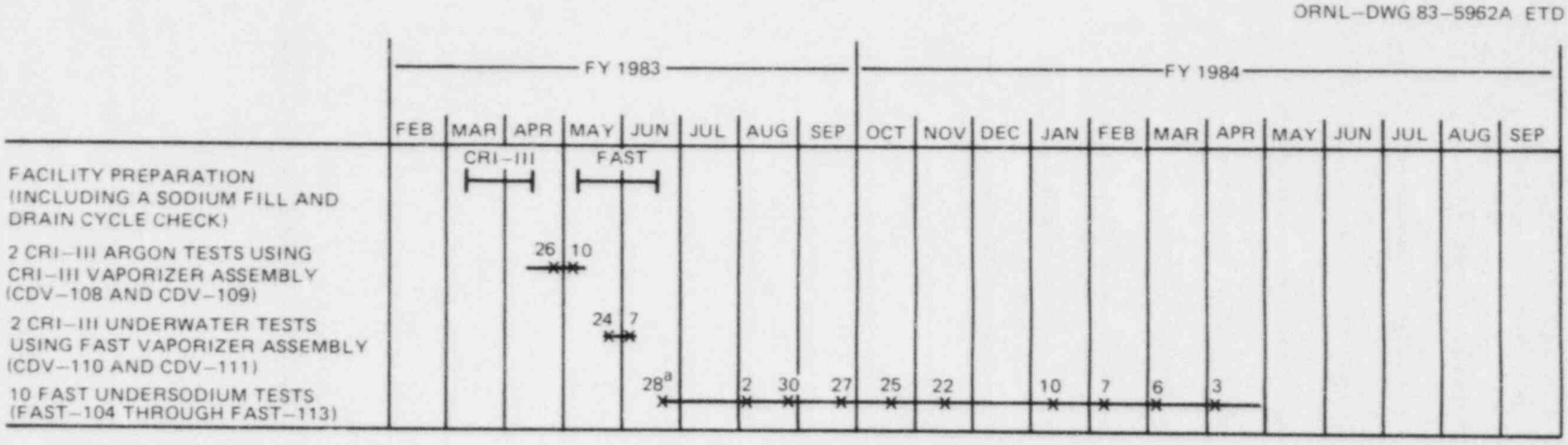

[a]REPEAT OF FAST-103 TEST.

Fig. 1. Schedule for FAST/CRI-III tests.

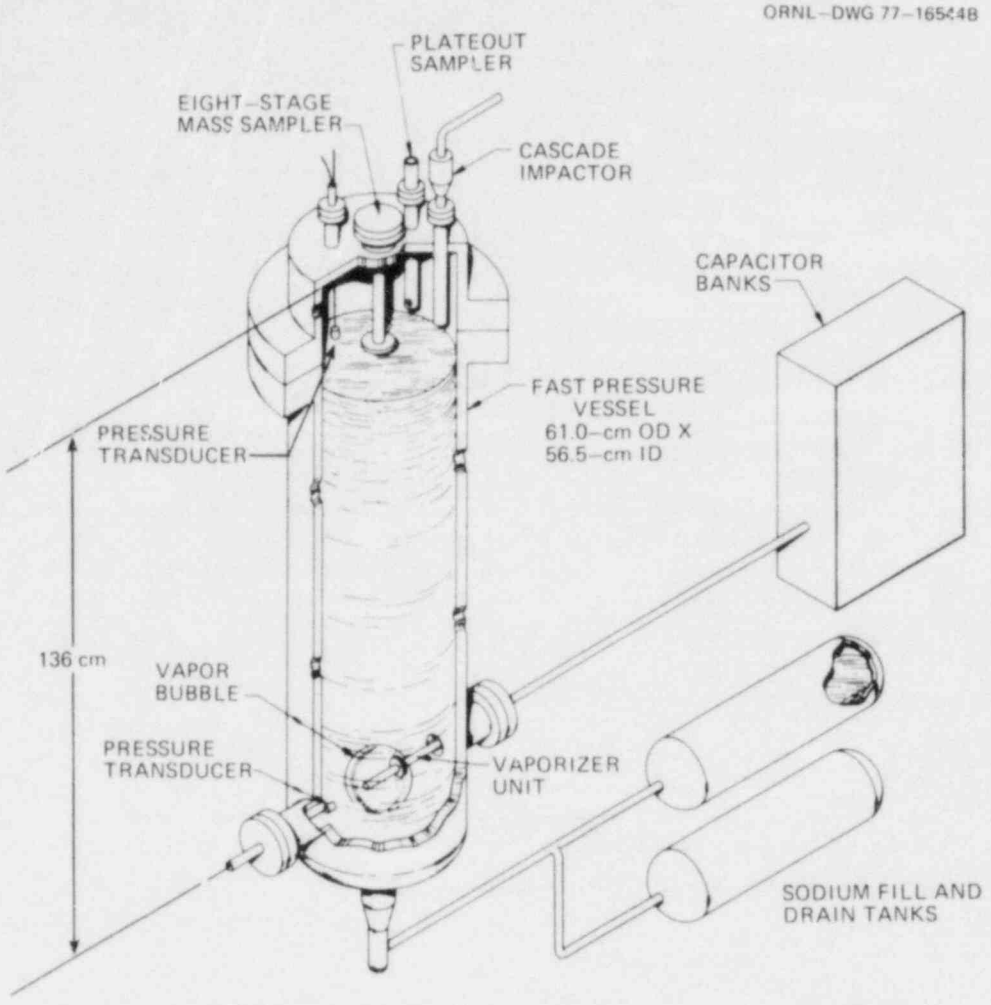

Fig. 2. Schematic of FAST test vessel.

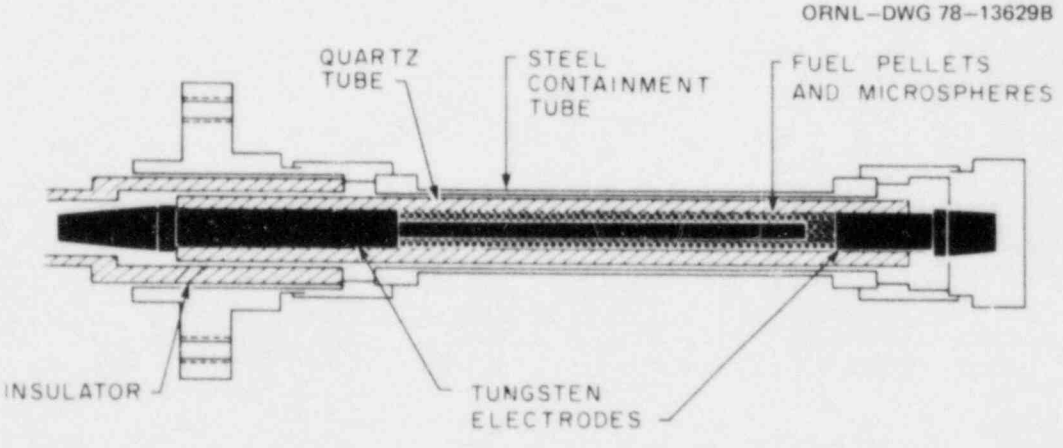

Fig. 3. Schematic of test sample used in underwater and undersodium tests. (Steel tube that surrounds quartz tube has a 19.6-mm OD and wall thickness of 0.13 mm. Quartz containment tube is 17.1-mm OD by 9.71-mm ID, and fuel pellet column is 4.86-mm diam by ~90 mm long.)

Table 1. FAST single-pin undersodium test plan[a]

FAST test No.	Pressure [kPa (abs)]		Nominal[b] sodium height above fuel specimen centerline (cm)	Objective
	Argon cover gas	Xenon fuel sample		
104	120	135	107	Repeat of FAST 103 Compare with previous results
105	120	340	107	Determine effect of changing xenon pressure
106	120	340	20	Determine effect of changing sodium height
107	120	340	10	Same as 106
108	120	340	5	Same as 106
109	300	340	5	Determine effect of changing sodium height at a second cover-gas pressure level
110	300	340	10	Same as 109
111	120	340	−30	Determine aerosol behavior over sodium at 540°C Verify aerosol sampling technique
112	300	340	20	Same as 109
113	300	340	107	Same as 109

[a]In all tests, the pressure vessel and sodium temperature will be 540°C.

[b]See Table 3 for actual sodium heights.

Table 2. Test specimen data

Test No.	UO_2			Quartz tube dimension (mm)	
	Pellet stack		Microsphere mass (g)		
	Mass (g)	Length (mm)		ID	OD
CDV-108	17.35	90.2	32.05	9.72	17.15
CDV-109	17.35	90.2	32.77	9.70	17.15
CDV-110	17.27	89.7	30.66	9.70	17.15
CDV-111	17.41	90.4	32.69	9.72	17.15
FAST-103[a]	17.36	90.4	32.93	9.70	17.15
FAST-104	17.58	91.7	32.39	9.70	17.15
FAST-105	17.49	91.2	32.06	9.70	17.15
FAST-106	17.59	91.4	31.97	9.70	17.15
FAST-107	17.50	91.1	31.48	9.70	17.15
FAST-108	17.36	90.3	31.68	9.70	17.15
FAST-109	17.66	91.9	31.86	9.70	17.15
FAST-110	17.63	91.5	32.08	9.70	17.15
FAST-111	17.57	91.5	31.99	9.73	17.15
FAST-112	17.44	90.7	31.84	9.73	17.15

[a]Included for comparison. FAST-103 was performed on December 15, 1981, prior to a 1-year shutdown of the facilities.

Table 3. Test conditions

Test No.	Type	Temperature (°C)	Argon cover gas		Fuel sample pressure at start of low preheat [kPa (abs)]	Liquid	
			Volume (m^3)	Pressure [kPa (abs)]		Volume (m^3)	Height above fuel specimen centerline (cm)
CDV-108	Argon	Room	0.56	120	120	0	
CDV-109	Argon	Room	0.56	120	120	0	
CDV-110	Underwater	Room	0.53	120	134	0.034	20
CDV-111	Underwater	Room	0.54	120	134	0.023	5.0
FAST-103[a]	Undersodium	540	0.092	120	134	0.37	105
FAST-104	Undersodium	540	0.090	120	133	0.37	106
FAST-105	Undersodium	540	0.095	120	341	0.37	104
FAST-106	Undersodium	540	0.30	120	340	0.16	24[b]
FAST-107	Undersodium	540	0.32	121	341	0.14	14[b]
FAST-108	Undersodium	540	0.34	120	340	0.12	7.7
FAST-109	Undersodium	540	0.33	300	341	0.13	9.5
FAST-110	Undersodium	540	0.32	300	340	0.14	14
FAST-111	Oversodium	540	0.45	122	341	0.014	−30
FAST-112	Undersodium	540	0.30	300	338	0.16	25

[a]Included for comparison. FAST-103 was performed on December 15, 1981, prior to a 1-year shutdown of the facilities.

[b]Sodium height previously reported[1] was revised based on the results of a comparison of the normal "Twin-I" tube continuous sodium level indication with recent independent (and presumably more accurate) continuity-probe measurements in the range of sodium heights between 3 and 15 cm.

Table 4. Electrical energy input data

Test No.	Preheat power (W)		Resistance at end of high preheat (Ω)	Time delay between high preheat and CDV (s)	Energy stored in capacitor banks (kJ)	CDV time to arcing (ms)	CDV energy input to arcing (kJ)
	Low	High					
CDV-108	500	1700	0.45	2.0	77.3	4.96	50.5
CDV-109	500	1700	0.52	2.0	76.9	3.26	33.0
CDV-110	500	1700	0.44	2.0	76.9	2.60	30.9
CDV-111	500	1700	0.45	2.0	76.5	3.26	35.6
FAST-103[a]	600	1600	0.43	2.0	76.5	3.15	37.9
FAST-104	600	1600	0.44	2.0	76.5	3.14	37.4
FAST-105	600	1600	0.41	2.0	76.9	2.61	32.2
FAST-106	600	1600	0.41	2.0	76.9	2.98	37.6
FAST-107	600	1600	0.46	2.0	76.5	2.30	28.8
FAST-108	600	1600	0.39	2.0	76.9	1.55	19.6
FAST-109	600	1600	0.40	2.0	76.5	1.65	20.3
FAST-110	540	1600	0.40	2.0	76.5	2.35	28.2
FAST-111	500	1550	0.41	2.0	77.3	1.93	22.8
FAST-112	540	1600	0.40	2.0	76.5	2.16	26.5

[a]Included for comparison. FAST-103 was performed on December 15, 1981, prior to a 1-year shutdown of the facilities.

partially melt the fuel pellets and reduce the resistance of the fuel sample to a level where the energy stored in the capacitor banks can be discharged in a few milliseconds at ~10-MW power to raise the energy level of the fuel to ~3 kJ/g by the time fuel sample disassembly occurs.

Test results obtained during this report period are presented in the following section.

2.1.2 Discussion of FAST undersodium test results

The experimental results obtained during this period related to fuel bubble behavior and aerosol transport to the cover-gas region in the FAST undersodium tests are presented in Sects. 2.1.2.1 and 2.1.2.2.

2.1.2.1 Fuel bubble behavior. Pressures are measured in the sodium and the cover gas to monitor the fuel bubble pressure and size vs time and the period of oscillation of the bubble (time between repetitive bubble expansions and contractions in the closed system). Preliminary modeling calculations have indicated that the pressure at the measurement point in the sodium (23 cm from the test sample centerline) is close to the fuel bubble pressure (within about 25% during the first bubble oscillation) in tests conducted at the sodium height of 107 cm, but follows the bubble pressure less closely at the lower sodium heights of 20 and 10 cm.

The sodium and cover-gas pressure transducer signals are captured on a dual-channel digital storage oscilloscope having a fast transient storage capability of 2048 points/channel; the signals are later transferred to permanent storage on flexible disks. A speed setting of 50 μs/point is normally chosen to give ~100-ms time coverage from the trigger point at the start of capacitor discharge. The sensors have a rated pressure range and frequency response of 3,450 kPa and 12,270 Hz for the sodium transducer and 345 kPa and 4,350 Hz for the cover-gas transducer. In situ calibration checks are made at the time of each test.

Pressure measurements made in the FAST-108 test are compared in Fig. 4 with those reported previously for the FAST-105 and FAST-107 tests;[1] expanded views of the sodium and cover-gas pressure traces are shown in Figs. 5 and 6, respectively. The times between the peaks in the sodium pressure traces in FAST-105 and FAST-107 (Fig. 5) indicate the bubble oscillation periods τ. The bubble oscillation pattern in the sodium pressure trace in FAST-108 is not as clear. Based on the observations made in the earlier underwater tests[4] (i.e., it appeared in the high-speed movies that the fuel bubble penetrated 5 cm of water in CDV-111), one might expect the fuel bubble to have penetrated the surface at a sodium height somewhat greater than 5 cm. However, there are many differences between the two sets of test conditions and coolants that can influence fuel bubble behavior, such as differences in the amount of coolant subcooling, coolant pool size, thermal conductivity, surface tension, emissivity, and density; even sodium-UO_2 chemical reactions[5] may be important.

The peaks in the cover-gas pressure traces (Fig. 6) are much weaker than the peaks in the sodium pressure traces. In FAST-105, the cover-gas peaks correspond fairly well to bubble expansions to maximum size as indicated by the valleys in the sodium pressure trace, and the cover-gas

ORNL PHOTO 3222-84

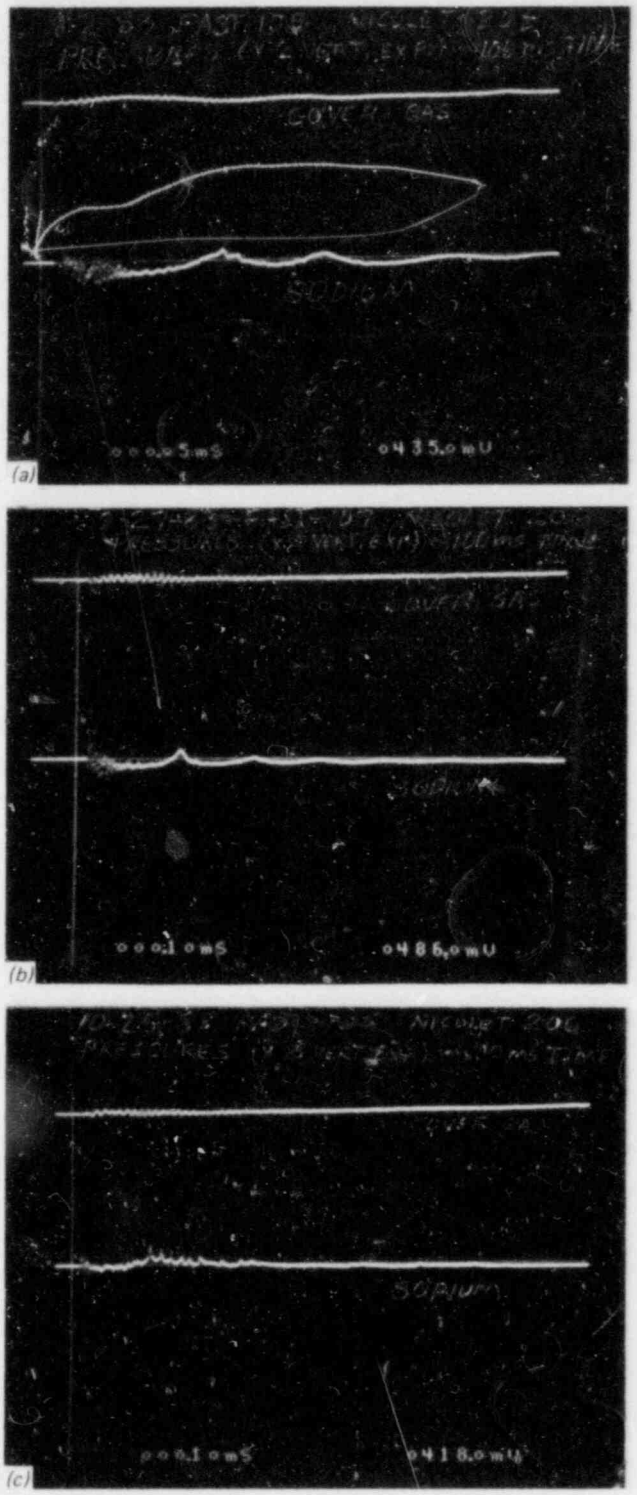

Fig. 4. Comparison of oscilloscope pressure traces in (*a*) FAST-105, (*b*) FAST-107, and (*c*) FAST-108.

ORNL PHOTO 3223–84

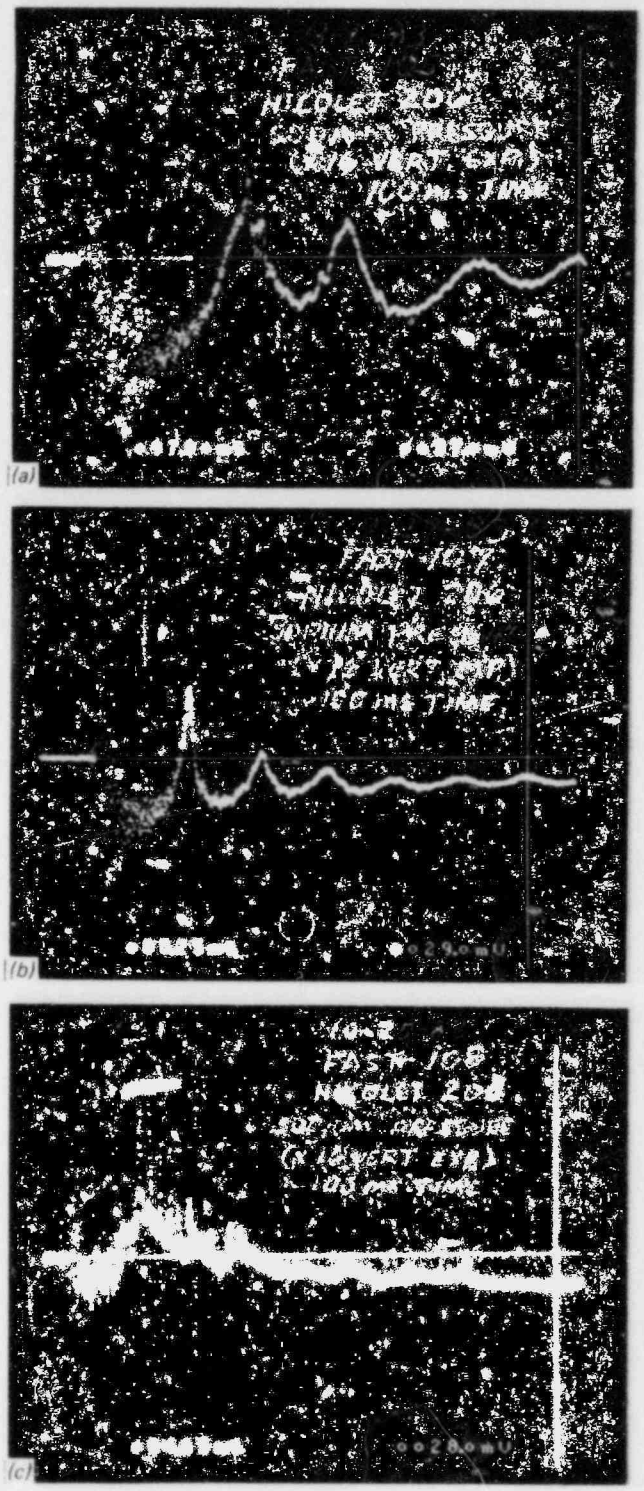

Fig. 5. Expanded views of oscilloscope sodium-pressure traces in (*a*) FAST-105, (*b*) FAST-107, and (*c*) FAST-108.

ORNL PHOTO 8224-84

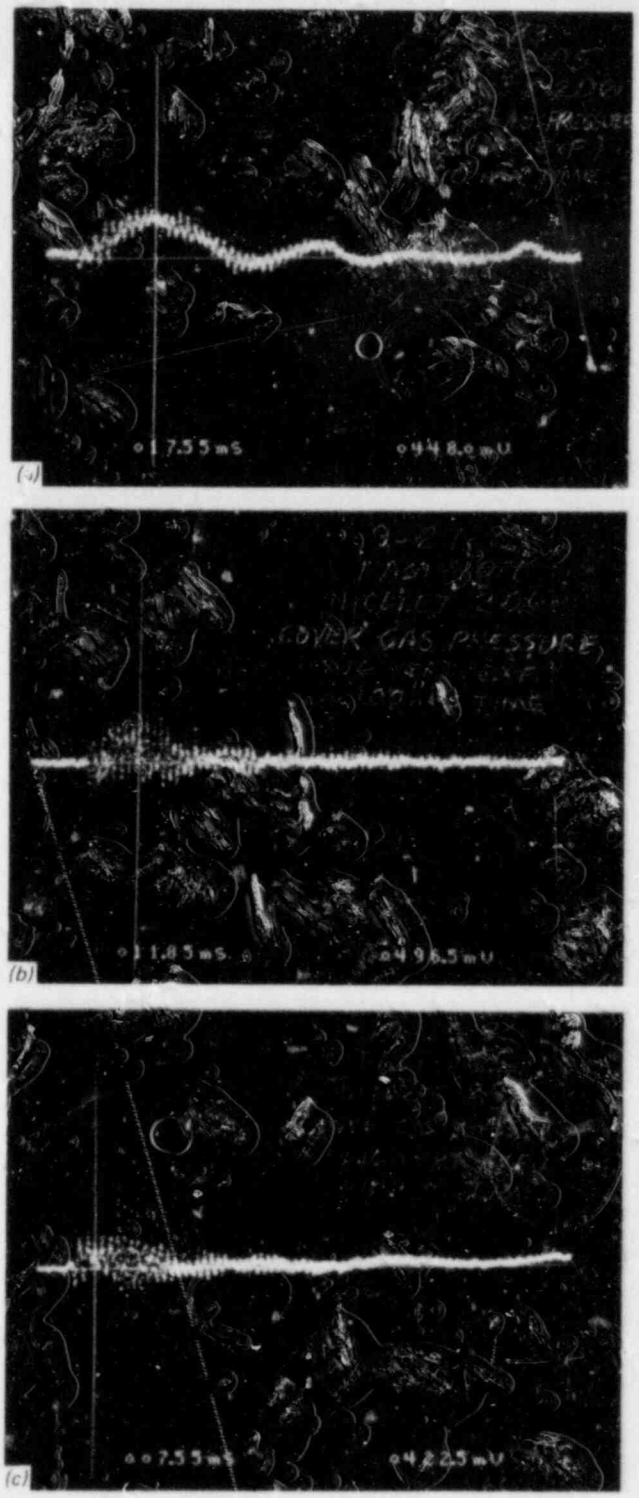

Fig. 6. Expanded views of oscilloscope cover-gas pressure traces in (*a*) FAST-105, (*b*) FAST-107, and (*c*) FAST-108.

pressure record can be used to estimate fuel bubble size vs time. The cover-gas pressure peaks in FAST-107 and FAST-108 are barely discernible because of loss of measurement sensitivity with the increased cover-gas volume and the increased noise in the signal.

Although no attempt has been made to associate the sodium pressure maximum and minimum points with possible fuel bubble expansion and contraction oscillations in FAST-108, the sodium pressure data are summarized in Table 5 so that the magnitude of pressure signals in Figs. 4 and 5 may be visualized. Similar tabulations of sodium pressure maximum and minimum points for FAST-105 through FAST-107 and of sodium and cover-gas pressure maximum points for FAST-104 and FAST-105 were given previously.[1]

Table 5. Sodium-pressure maximum and minimum points in FAST-108

Pressure point No.	Time from sample disassembly (ms)	Pressure indication above baseline value[a] (kPa)
Maximum		
1	0.5	64.6[b]
2	13.85	80.3[b]
Minimum		
1	6.35	−24[b]

[a]Baseline sodium pressure was 120 kPa (abs).

[b]Data contain large uncertainties because of noise in the signal.

The results of those tests showed a decreasing initial bubble oscillation period (τ_1) from 32 to 17 ms with decreasing sodium height above the fuel sample from 104 to 14 cm for the tests at 120-kPa (abs) argon cover-gas pressure. Sodium pressure increases up to 1.2 MPa were measured, and bubble radii up to ~10 cm were indicated by the cover-gas pressure increases.

Oscilloscope traces of the pressure records obtained in the tests conducted at the higher cover-gas pressure of 300 kPa (abs) (FAST-109, FAST-110, and FAST-112) are shown in Figs. 7 and 8 for the sodium and cover-gas pressures, respectively; the sodium pressure data are summarized in Table 6. As evident from comparing the sodium pressure traces in Fig. 7 with those in Fig. 5, the indicated bubble oscillation periods are much shorter at the higher cover-gas pressure. Comparison of times between sodium pressure peaks in Table 6 with those in Table 5 for FAST-108 and those reported earlier for FAST-106 and FAST-107 (Table 5, Ref. 1)

ORNL PHOTO 3225–84

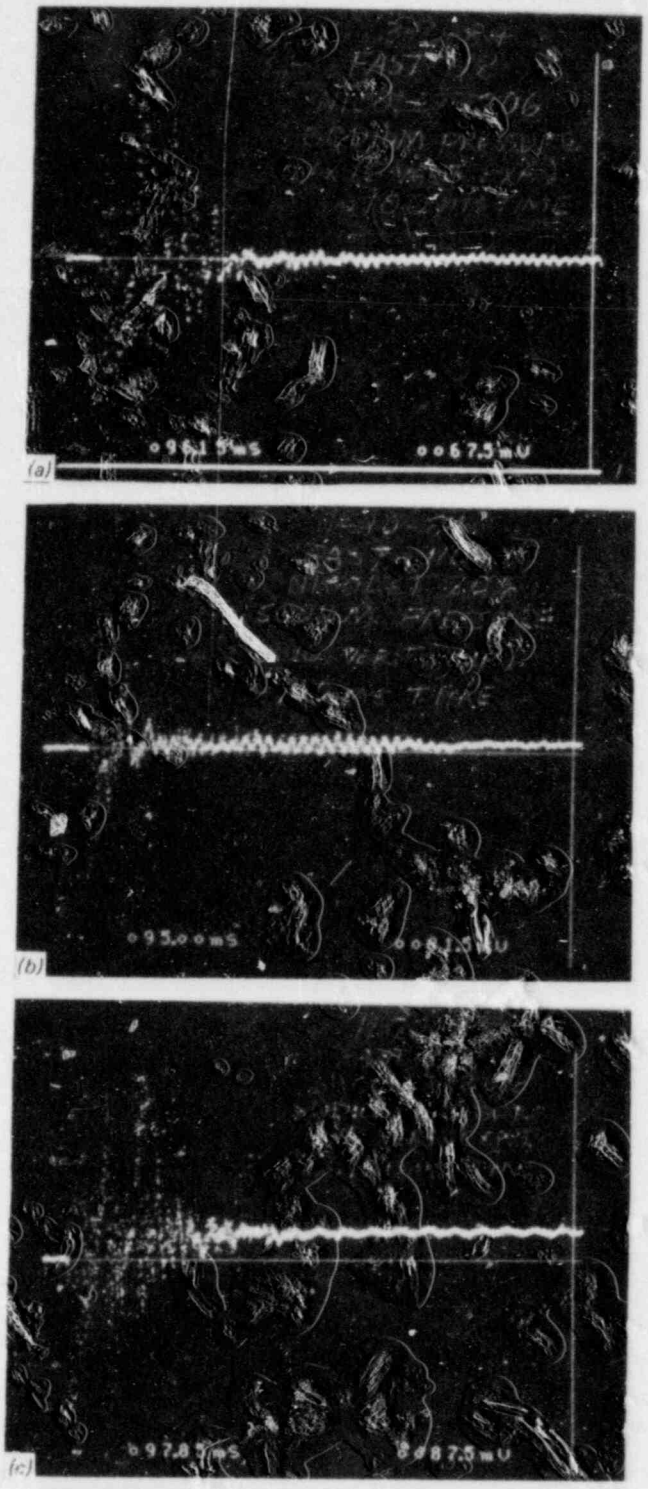

Fig. 7. Expanded views of oscilloscope sodium-pressure traces in (*a*) FAST-112, (*b*) FAST-110, and (*c*) FAST-109.

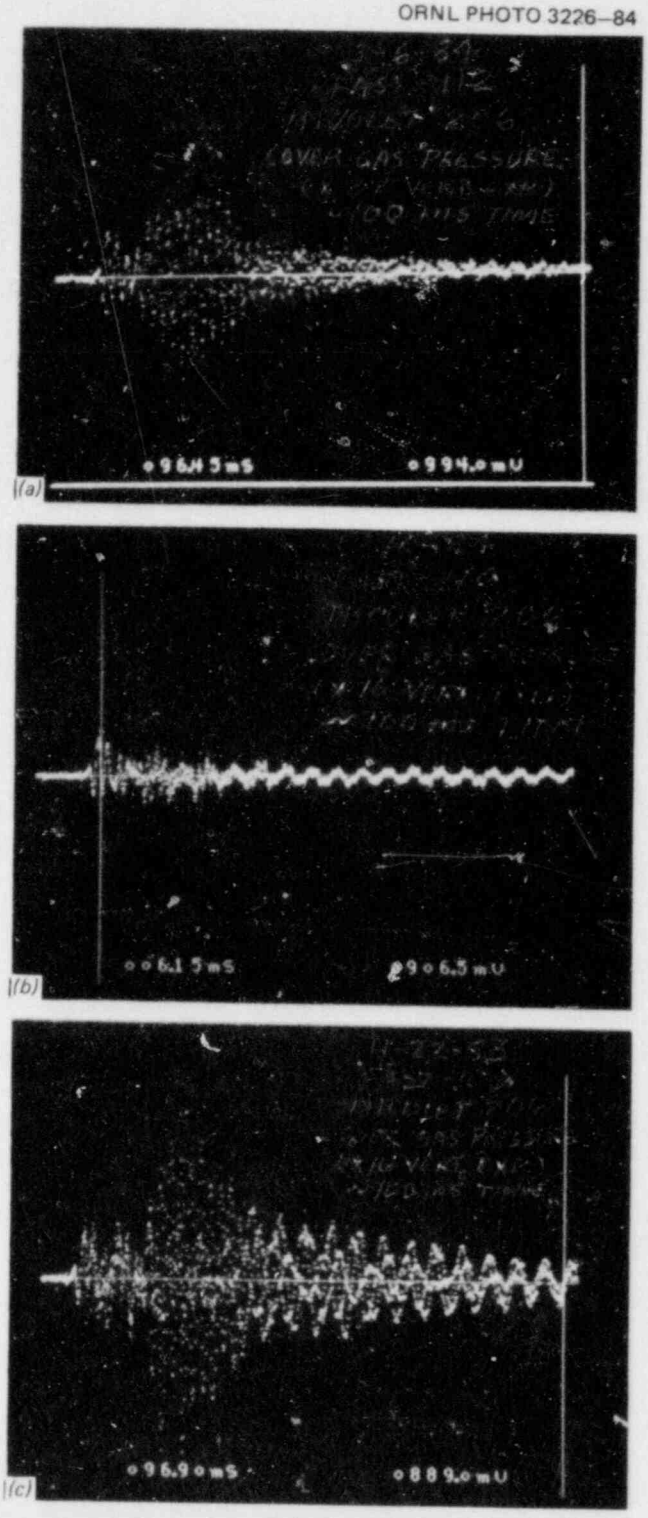

Fig. 8. Expanded views of oscilloscope cover-gas pressure traces in (*a*) FAST-112, (*b*) FAST-110, and (*c*) FAST-109.

Table 6. Sodium-pressure maximum and minimum points from FAST-112, FAST-110, and FAST-109

(Effects of energy input level[a] and decreasing sodium height H are shown)

Pressure point No.	Time from sample disassembly (ms)			Pressure indication above baseline value[b] (kPa)		
	FAST-112 (H = 25 cm)	FAST-110 (H = 14 cm)	FAST-109 (H = 9.5 cm)	FAST-112 (H = 25 cm)	FAST-110 (H = 14 cm)	FAST-109 (H = 9.5 cm)
Maximum						
1	0.54	0.60	0.95	350	161[c]	360[c]
2	7.89	7.05	7.05	293	86	191
3	13.94	11.50	13.00	162	34	214[c]
4	18.29			83		
5	22.09			56		
Minimum						
1	3.69	3.80	4.10	−111	−23[c]	−45
2	11.29	9.35	10.30	−103	−13	−17

[a]Capacitor discharge energy input to arcing was 26.5 kJ in FAST-112, 28.2 kJ in FAST-110, and 20.3 kJ in FAST-109.

[b]Baseline sodium pressure was 301 kPa (abs) in FAST-112 and FAST-109, and 300 kPa (abs) in FAST-110.

[c]Data contain large uncertainties because of noise in the signal.

shows that the periods at the higher cover-gas pressure of 300 kPa (abs) range from about one-half to one-third of those measured at the lower cover-gas pressure of 120 kPa (abs). Preliminary modeling calculations indicated that the initial bubble oscillation period at the higher pressure would be slightly less than one-half that at the lower pressure for a sodium height of 107 cm. The reason for the greater than usual noise in the cover-gas pressure signals in FAST-109 and FAST-112 (Fig. 8) is unknown.

Pressure measurements were also obtained in FAST-111, but they are of less interest than in the other tests, because the sodium level was 30 cm *below* the fuel specimen (see Table 1) and the lower pressure transducer (at the elevation of the fuel specimen) was above the sodium surface instead of in the sodium pool.

2.1.2.2 Aerosol transport. A series of aerosol samples of the cover gas was obtained in each test starting soon after capacitor discharge (time = 0). The sampling procedure consists of drawing a measured amount of cover gas through a collection filter located inside the vessel at the lower end of the eight-stage mass sampler. After the test, the filters are analyzed for uranium content (and other chemical species) by the ORNL Analytical Chemistry Division. The filter being used in the sodium tests is a 28.5-mm-diam by 1.6-mm-thick, 2-μm pore-size sintered stainless steel (Type 316) disk.

Aerosol sampling results for FAST-104 through FAST-112 are given in Tables 7–15, respectively. The results show a surprisingly strong attenuation of the aerosol release by low heights of sodium over the horizontal test sample. Because of this unexpected result, the original test plan was modified to include the FAST-111 test (see Table 1) in an

Table 7. Aerosol sampling results for FAST-104

Aerosol samplers used: mass (eight-stage)

Cover-gas volume: 0.090 m^3

Aerosol data:

Sample No.	Time after fuel specimen disassembly (min)	Uranium concentration		Airborne uranium mass corrected for depletion[a] (g U)
		Measured (g U/m^3)	Corrected for depletion[a] (g U/m^3)	
1	3.3	3.9×10^{-4}	3.9×10^{-4}	3.5×10^{-5}
2	5.4	5.6×10^{-4}	5.9×10^{-4}	5.3×10^{-5}
3	8.6	2.4×10^{-3}	2.7×10^{-3}	2.5×10^{-4}
4	12.5	6.4×10^{-4}	7.6×10^{-4}	6.9×10^{-5}
5	16.1	3.4×10^{-4}	4.4×10^{-4}	4.0×10^{-5}
6	26.5	6.5×10^{-4}	9.0×10^{-4}	8.2×10^{-5}
7	38.6	3.7×10^{-4}	5.5×10^{-4}	5.0×10^{-5}

Initial uranium concentration:[b] $\sim 1.1 \times 10^{-3}$ g U/m^3

Initial airborne uranium mass:[b] $\sim 10^{-4}$ g U

[a]Corrected for the loss from the cover gas of uranium collected on the filters (i.e., the amount that would have been present in the cover gas had no samples been taken).

[b]Extrapolation of these data back to the time of fuel specimen disassembly contains large uncertainty, because these data are near the lower limit of detection and contain considerable scatter.

Table 8. Aerosol sampling results for FAST-105

Aerosol samplers used: mass (eight-stage)

Cover-gas volume: 0.095 m^3

Aerosol data:

Sample No.	Time after fuel specimen disassembly (min)	Uranium concentration		Airborne uranium mass corrected for depletion[a] (g U)
		Measured (g U/m^3)	Corrected for depletion[a] (g U/m^3)	
2	3.5	1.2×10^{-2}	1.2×10^{-2}	1.2×10^{-3}
3	5.3	7.3×10^{-3}	7.7×10^{-3}	7.2×10^{-4}
4	8.4	1.6×10^{-3}	1.7×10^{-3}	1.6×10^{-4}

Initial uranium concentration:[b]

Initial airborne uranium mass:[b]

[a]Corrected for the loss from the cover gas of uranium collected on the filters (i.e., the amount that would have been present in the cover gas had no samples been taken).

[b]Too few data points for good extrapolation back to the time of fuel specimen disassembly.

Table 9. Aerosol sampling results for FAST-10b

Aerosol samplers used: mass (eight-stage)

Cover-gas volume: 0.30 m^3

Aerosol data:

Sample No.	Time after fuel specimen disassembly (min)	Uranium concentration		Airborne uranium mass corrected for depletion[a] (g U)
		Measured (g U/m^3)	Corrected for depletion[a] (g U/m^3)	
1	3.1	3.9×10^{-4}	3.9×10^{-4}	1.2×10^{-4}
2	5.3	2.6×10^{-4}	2.7×10^{-4}	8.0×10^{-5}
3	8.7	2.6×10^{-4}	2.7×10^{-4}	8.1×10^{-5}
4	11.5	2.0×10^{-4}	2.1×10^{-4}	6.3×10^{-5}
6	26.0	2.5×10^{-4}	2.8×10^{-4}	8.3×10^{-5}

Initial uranium concentration:[b] $\sim 5.0 \times 10^{-4}$ g U/m^3

Initial airborne uranium mass:[b] $\sim 1.5 \times 10^{-4}$ g U

[a]Corrected for the loss from the cover gas of uranium collected on the filters (i.e., the amount that would have been present in the cover gas had no samples been taken).

[b]Extrapolation of these data back to the time of fuel specimen disassembly contains large uncertainty, because these data are near the lower limit of detection and contain considerable scatter.

Table 10. Aerosol sampling results for FAST-10?

Aerosol samplers used: mass (eight-stage)

Cover-gas volume: 0.32 m^3

Aerosol data:

Sample No.	Time after fuel specimen disassembly (min)	Uranium concentration		Airborne uranium mass corrected for depletion[a] (g U)
		Measured (g U/m^3)	Corrected for depletion[a] (g U/m^3)	
1	3.3	1.2×10^{-3}	1.2×10^{-3}	3.7×10^{-4}
2	5.5	1.1×10^{-3}	1.1×10^{-3}	3.5×10^{-4}
3	8.3	9.8×10^{-4}	1.0×10^{-3}	3.3×10^{-4}
4	12.1	9.1×10^{-4}	9.5×10^{-4}	3.1×10^{-4}
5	16.1	8.3×10^{-4}	8.8×10^{-4}	2.8×10^{-4}
6	25.7	7.1×10^{-4}	7.6×10^{-4}	2.5×10^{-4}
7	35.5	6.4×10^{-4}	7.0×10^{-4}	2.3×10^{-4}

Initial uranium concentration: $\sim 1.5 \times 10^{-3}$ g U/m^3

Initial airborne uranium mass: $\sim 4.7 \times 10^{-4}$ g U

[a]Corrected for the loss from the cover gas of uranium collected on the filters (i.e., the amount that would have been present in the cover gas had no samples been taken).

Table 11. Aerosol sampling results for FAST-108

Aerosol samplers used: mass (eight-stage)

Cover-gas volume: 0.34 m^3

Aerosol data:

Sample No.	Time after fuel specimen disassembly (min)	Uranium concentration		Airborne uranium mass corrected for depletion[a] (g U)
		Measured (g U/m^3)	Corrected for depletion[a] (g U/m^3)	
1	4.4	4.2×10^{-4}	4.2×10^{-4}	1.4×10^{-4}
2	6.2	4.9×10^{-4}	5.0×10^{-4}	1.7×10^{-4}
3	8.6	6.4×10^{-4}	6.5×10^{-4}	2.2×10^{-4}
4	12.5	5.7×10^{-4}	6.0×10^{-4}	2.0×10^{-4}
5	21.1	4.5×10^{-4}	4.7×10^{-4}	1.6×10^{-4}
6	36.2	3.9×10^{-4}	4.2×10^{-4}	1.4×10^{-4}
7	51.5	3.2×10^{-4}	3.5×10^{-4}	1.2×10^{-4}

Initial uranium concentration:[b] ~9.7×10^{-4} g U/m^3

Initial airborne uranium mass:[b] ~3.3×10^{-4} g U

[a]Corrected for the loss from the cover gas of uranium collected on the filters (i.e., the amount that would have been present in the cover gas had no samples been taken).

[b]Extrapolation of these data back to the time of fuel specimen disassembly contains large uncertainty, because these data are near the lower limit of detection and contain considerable scatter.

Table 12. Aerosol sampling results for FAST-109

Aerosol samplers used: mass (eight-stage)

Cover-gas volume: 0.33 m^3

Aerosol data:

Sample No.	Time after fuel specimen disassembly (min)	Uranium concentration		Airborne uranium mass corrected for depletion[a] (g U)
		Measured (g U/m^3)	Corrected for depletion[a] (g U/m^3)	
1	3.7	1.8×10^{-4}	1.8×10^{-4}	6.1×10^{-5}
2	5.3	2.1×10^{-4}	2.1×10^{-4}	7.2×10^{-5}
3	8.1	6.4×10^{-4}	6.5×10^{-4}	2.2×10^{-4}
4	12.3	4.8×10^{-4}	5.0×10^{-4}	1.7×10^{-4}
5	20.3	7.2×10^{-4}	7.5×10^{-4}	2.5×10^{-4}
6	36.8	1.5×10^{-4}	1.5×10^{-4}	5.1×10^{-5}

Initial uranium concentration:[b] ~1.1×10^{-3} g U/m^3

Initial airborne uranium mass:[b] ~3.5×10^{-4} g U

[a]Corrected for the loss from the cover gas of uranium collected on the filters (i.e., the amount that would have been present in the cover gas had no samples been taken).

[b]Extrapolation of these data back to the time of fuel specimen disassembly contains large uncertainty, because these data are near the lower limit of detection and contain considerable scatter.

Table 13. Aerosol sampling results for FAST-110

Aerosol samplers used: mass (eight-stage)

Cover-gas volume: 0.32 m^3

Aerosol data:

Sample No.	Time after fuel specimen disassembly (min)	Uranium concentration		Airborne uranium mass corrected for depletion[a] (g U)
		Measured (g U/m^3)	Corrected for depletion[a] (g U/m^3)	
1	2.9	5.4×10^{-4}	5.4×10^{-4}	1.7×10^{-4}
2	5.1	4.1×10^{-4}	4.1×10^{-4}	1.3×10^{-4}
3	8.7	4.6×10^{-4}	4.7×10^{-4}	1.5×10^{-4}
4	12.1	2.5×10^{-4}	2.6×10^{-4}	8.3×10^{-5}
6	21.3	2.7×10^{-4}	2.8×10^{-4}	8.9×10^{-5}
7	35.9	2.4×10^{-4}	2.5×10^{-4}	8.1×10^{-5}
8	53.4	2.3×10^{-4}	2.4×10^{-4}	7.9×10^{-5}

Initial uranium concentration:[b] ~6.9×10^{-4} g U/m^3

Initial airborne uranium mass:[b] ~2.2×10^{-4} g U

[a]Corrected for the loss from the cover gas of uranium collected on the filters (i.e., the amount that would have been present in the cover gas had no samples been taken).

[b]Extrapolation of these data back to the time of fuel specimen disassembly contains large uncertainty, because these data are near the lower limit of detection and contain considerable scatter.

Table 14. Aerosol sampling results for FAST-111

Aerosol samplers used: mass (eight-stage)

Cover-gas volume: 0.45 m^3

Aerosol data:

Sample No.	Time after fuel specimen disassembly (min)	Uranium concentration		Airborne uranium mass corrected for depletion[a] (g U)
		Measured (g U/m^3)	Corrected for depletion[a] (g U/m^3)	
1	2.3	2.7	2.7	1.2
2	4.6	2.4	2.4	1.1
3	9.2	1.7	1.8	0.78
4	12.8	1.6	1.7	0.75
5	20.6	1.4	1.4	0.64
6	35.1	0.94	1.0	0.45
7	51.0	0.64	0.69	0.31

Initial uranium concentration: 3.1 g U/m^3

Initial airborne uranium mass: 1.4 g U

[a]Corrected for the loss from the cover gas of uranium collected on the filters (i.e., the amount that would have been present in the cover gas had no samples been taken).

Table 15. Aerosol sampling results for FAST-112

Aerosol samplers used: mass (eight-stage)

Cover-gas volume: 0.30 m^3

Aerosol data:

Sample No.	Time after fuel specimen disassembly (min)	Uranium concentration		Airborne uranium mass corrected for depletion[a] (g U)
		Measured (g U/m^3)	Corrected for depletion[a] (g U/m^3)	
1	2.6	5.0×10^{-4}	5.0×10^{-4}	1.5×10^{-4}
2	4.4	2.3×10^{-3}	2.4×10^{-3}	7.0×10^{-4}
3	8.5	2.5×10^{-3}	2.6×10^{-3}	7.7×10^{-4}
4	12.5	1.0×10^{-3}	1.0×10^{-3}	3.1×10^{-4}
5	20.7	5.0×10^{-4}	5.2×10^{-4}	1.6×10^{-4}
6	35.7	7.1×10^{-4}	7.5×10^{-4}	2.2×10^{-4}
7	50.7	4.1×10^{-4}	$4.4 \times 10_{-4}$	1.3×10^{-4}

Initial uranium concentration:[b] ~3.1×10^{-3} g U/m^3

Initial airborne uranium mass:[b] ~9.3×10^{-4} g U

[a]Corrected for the loss from the cover gas of uranium collected on the filters (i.e., the amount that would have been present in the cover gas had no samples been taken).

[b]Extrapolation of these data back to the time of fuel specimen disassembly contains large uncertainty, because these data are near the lower limit of detection and contain considerable scatter.

attempt to demonstrate beyond question that fuel aerosol could be detected and measured in the presence of sodium vapor with the aerosol sampling techniques used in the previous tests. The expected amount of a greenish-brown material was collected on the filters in FAST-111, and the sampling results (Table 14) were in good agreement with the results of earlier high-temperature tests in an argon atmosphere[6] (FAST-13 through FAST-15). Thus, the FAST-111 results support the very low aerosol releases measured in the other undersodium tests and the adequacy of the aerosol sampling techniques. By comparing the undersodium aerosol sampling results with the oversodium FAST-111 results (which represent an upper bound for the release that can be expected for the energy input level of the test), an estimate of the fraction of fuel vapor transported through the sodium to the cover gas may be obtained. As evident from the aerosol sampling results plotted in Figs. 9 and 10 for the tests conducted at the cover-gas pressures of 120 and 300 kPa (abs), respectively, less than 10^{-3} of the fuel vapor was found in the cover gas in each undersodium test, with no

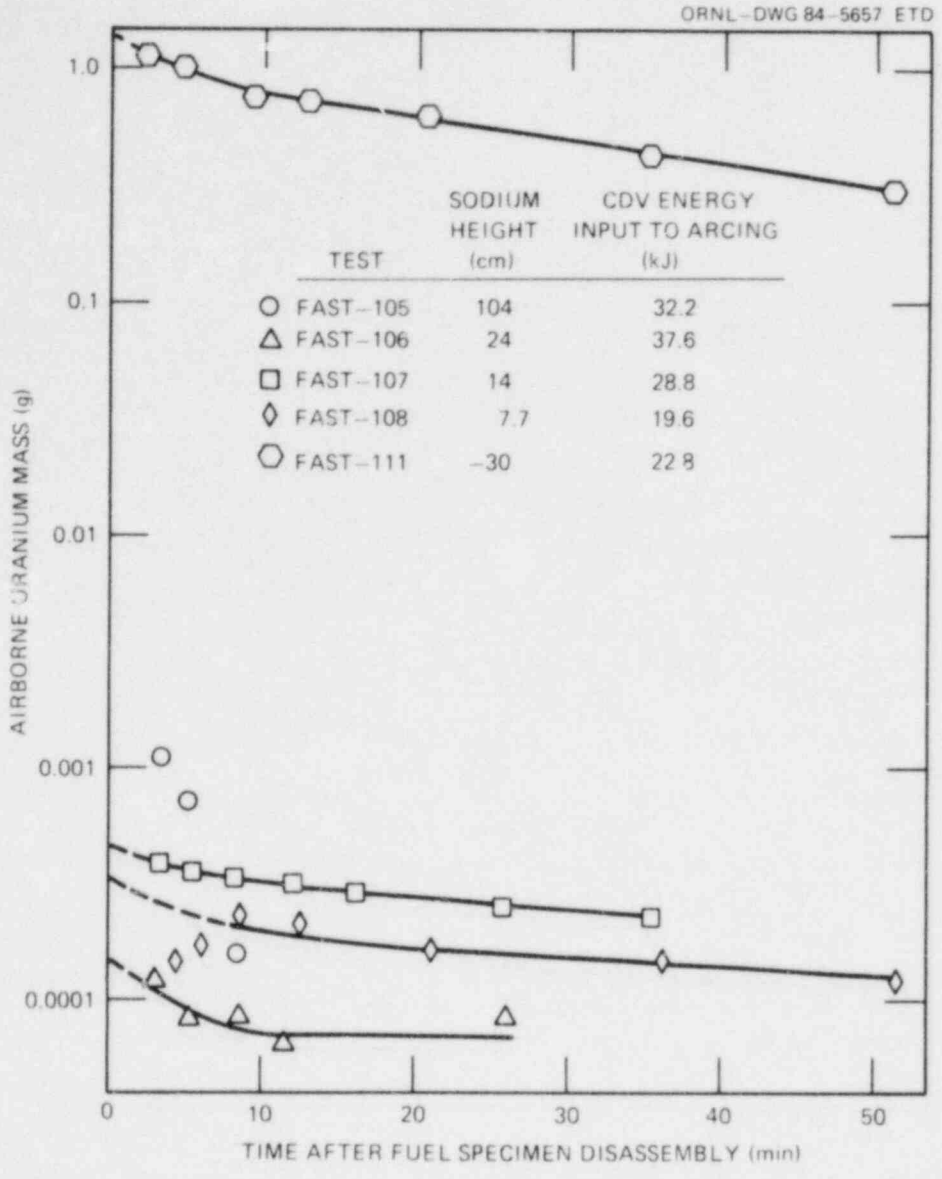

Fig. 9. Aerosol sampling results for FAST sodium tests conducted at argon cover-gas pressure of 1.0 kPa (abs) and xenon fuel sample pressure of 340 kPa (abs).

obvious increase with decreasing sodium height, even though the sodium height was varied from 106 to 8 cm above the centerline of the fuel sample. It should be emphasized that while these results show a strong attenuating effect on aerosol transport of even shallow depths of 540°C sodium, this effect should be considered specific to the FAST test vessel and experimental conditions.

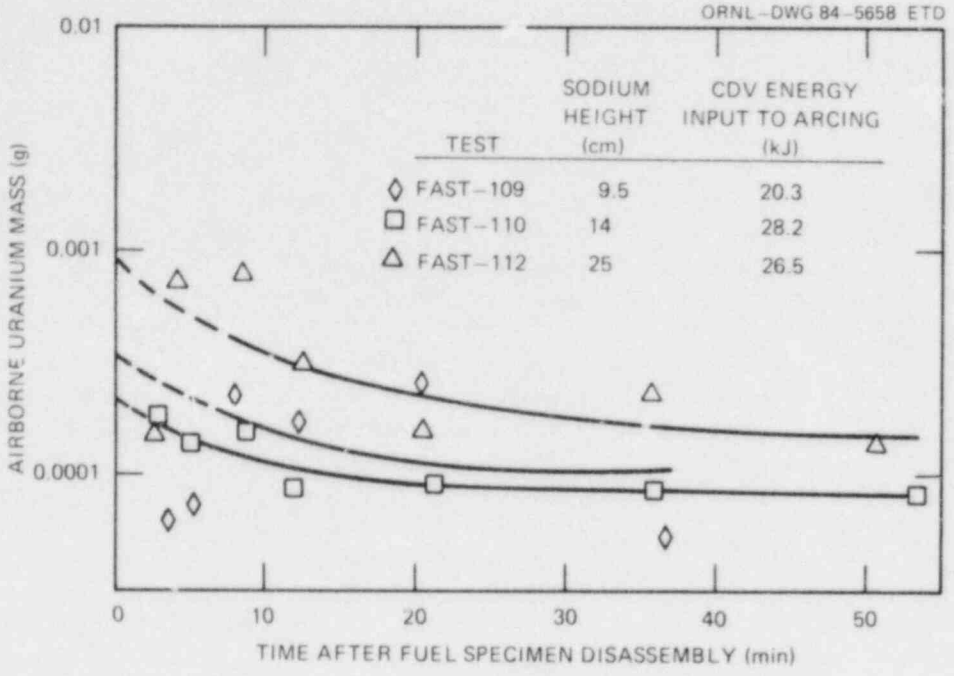

Fig. 10. Aerosol sampling results for FAST sodium tests conducted at argon cover-gas pressure of 300 kPa (abs) and xenon fuel sample pressure of 340 kPa (abs).

2.2 Secondary Containment Aerosol Studies in the NSPP

R. E. Adams M. T. Hurst
A. L. Johnson

2.2.1 Introduction

Studies continued on the behavior of aerosols assumed to be released into containment environments during LWR accident sequences. Previous quarterly progress reports contain results from single-component aerosol experiments with U_3O_8 aerosol, Fe_2O_3 aerosol, and concrete aerosol in both dry air and steam-air environments. More recently, attention is being given to the behavior of multicomponent aerosols; the first pair of aerosols to be studied is U_3O_8 + Fe_2O_3. Three experiments have been performed in a steam-air environment and one in a dry air environment. Details on NSPP experiments 613 and 631 are contained in this report; results from these experiments are compared with the results from previous experiments, NSPP experiments 611 and 612.

2.2.2 LWR aerosol experiment 613

Experiment 613 was the third in a series involving a mixed aerosol of Fe_2O_3 and U_3O_8. This mixture is a simulant for aerosols emanating

from molten fuel and molten-core support and structural materials. To prepare the test atmosphere, steam was introduced into the vessel, which was initially at 0.037 MPa (abs) and ambient temperature, to bring the vessel atmosphere (air) to an average temperature of 381 K and an absolute pressure of 0.178 MPa. This heating step required about 1.2 h; at this point, the rate of steam injection was reduced and the accumulated steam condensate in the bottom of the NSPP vessel was removed to a holding vessel. The two test aerosols were produced with separate plasma torch (PT) aerosol generators and mixed within the vessel. Fe_2O_3 aerosol was generated for a period of 26 min starting at time 0; the U_3O_8 aerosol generator was operated for 3 min starting at 13 min and ending at 16 min (measured from time 0). Steam injection at the low rate was maintained for ~6 h to balance steam losses at the vessel wall. Over this period, the temperature and pressure slowly increased until, at 6 h, the average temperature was 386 K and the pressure was 0.220 MPa (abs). The vessel was allowed to cool for 18 h after termination of steam injection.

Aerosol mass concentration. The two aerosols are injected into the vessel in the upper quadrant at two different locations, and the steam is introduced near the bottom of the vessel. To facilitate mixing of the two aerosols and the steam, a small fan-mixer is installed in the center of the vessel near the bottom. Operation of the fan-mixer produced a fairly homogeneous mixture of aerosol and steam as illustrated in Fig. 11, which contains the results for Fe_2O_3 aerosol from the four in-vessel filter samplers installed at four different locations within the vessel (see Table 16).

Table 16. Locations of NSPP aerosol mass concentration samplers

Sampler	Radial direction	Distance from bottom [m (ft)]	Radial distance from centerline [m (ft)]
In-vessel 151	East	4.15 (13.6)	0.58 (1.90)
In-vessel 152	Southeast	4.15 (13.6)	1.06 (3.48)
In-vessel 153	East	2.80 (9.2)	1.09 (3.58)
In-vessel 154	Southeast	1.34 (4.4)	1.11 (3.64)
Wall 155	South	4.15 (13.6)	0.61 (2.0)
Wall 156	Southeast	2.80 (9.2)	0.025 (1 in.) from wall
Wall 157	Southwest	2.80 (9.2)	1.06 (3.48)

The first set of aerosol mass concentration samples was taken at 24 min (2 min before termination of aerosol generation), and the aerosol mass concentration values were scattered indicating nonhomogeneous conditions. The second set of samples was taken at 34.4 min (8.4 min after

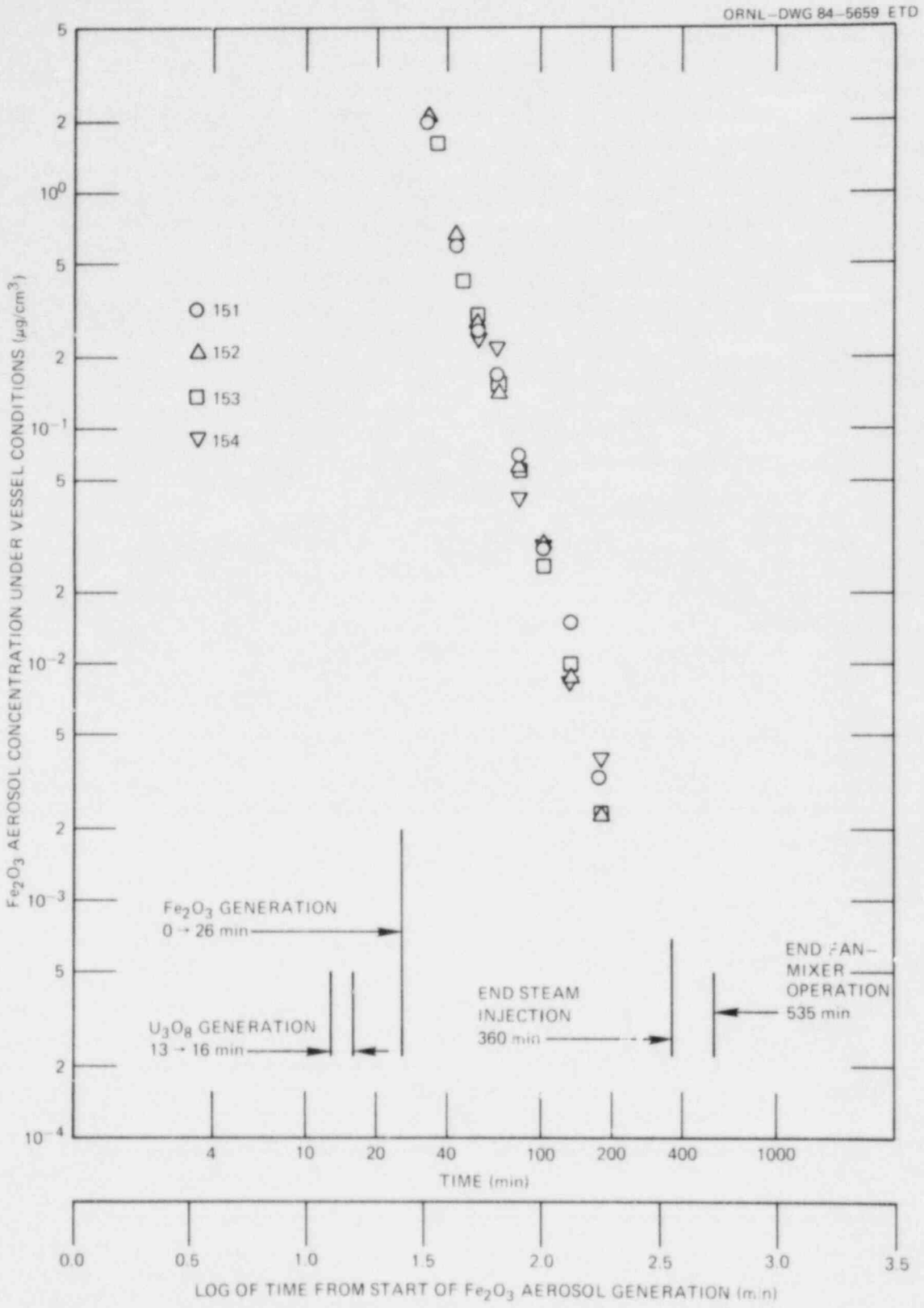

Fig. 11. Aerosol concentration (Fe_2O_3) as function of time in steam environment (NSPP No. 613).

termination of aerosol generation), and the values were comparable, indicating more complete mixing of the aerosol within the vessel. At this time, the average mass concentrations of Fe_2O_3 and U_3O_8 aerosol were 1.90 and 0.23 $\mu g/cm^3$, respectively. Extrapolation of these data to the time of Fe_2O_3 aerosol generator cutoff (26 min) yields values of 6.8 and 0.7 $\mu g/cm^3$ for Fe_2O_3 and U_3O_8 aerosol, respectively. The ratio of Fe_2O_3 to U_3O_8 was, therefore, 9.7 to 1, which is reasonably close to the target ratio of 10 to 1. The rate of disappearance of the two aerosols from the vessel environment is approximately the same as illustrated in Fig. 12; this behavior suggests that the two aerosols are coagglomerated.

Aerosol particle size. The aerodynamic mass median diameter (AMMD) of the aerosol was measured by both the spiral centrifuge sampler and the cascade impactor (Andersen Mark III). The "wet" aerosol was dried by dilution with clean air before introduction into the samplers. At 29.3 min after start of Fe_2O_3 aerosol generation, an AMMD of about 1.7 μm (σ_g = 1.7) for the mixed aerosol was determined by the spiral centrifuge sampler; at 138 min, an impactor sample indicated an AMMD of 1.0 μm (σ_g = 2.1) for the aerosol mixture. Determination of the AMMD by using only the Fe_2O_3 mass fraction or the U_3O_8 mass fraction yielded equivalent values for the AMMD in the previous two mixed aerosol experiments (Nos. 611 and 612). The same behavior was true in this experiment for the early centrifuge sample; in the later impactor sample, the U_3O_8 mass fraction produced an AMMD of 1.1 μm (σ_g = 3.3), however. In this later sample (138 min) the mass of sample taken was low, and this could account for the different behavior noted. On the whole, the sizing data suggest coagglomeration of the two aerosols.

Aerosol distribution. At the termination of the experiment (24 h), the approximate distribution of the mixed aerosol (Fe_2O_3 + U_3O_8), as determined by the total fallout samplers, the total plateout samplers, and the final filter sample was as follows: aerosol settled onto floor of vessel, 65%; aerosol plated onto internal surfaces, 35%; and aerosol still suspended in the vessel atmosphere, nil.

2.2.3 LWR aerosol experiment 631

This experiment involved study of the behavior of U_3O_8 and Fe_2O_3 aerosol in a dry air environment. Results from this test will serve to illustrate the magnitude of the influence of steam on mixed aerosol behavior as studied in Tests 611, 612, and 613.

The two aerosols were generated simultaneously with separate PT aerosol generators and mixed within the vessel. The initial test atmosphere was dry air at ambient temperature and pressure; the relative humidity was <20%. Fe_2O_3 aerosol was generated for a period of 16.2 min starting at time 0; the U_3O_8 aerosol was generated for a period of 4.3 min starting at elapsed time 11 min and ending at 15.3 min.

Aerosol mass concentration. Although this experiment did not involve steam, the small fan-mixer was operated in the same manner as in Tests 611-613 to promote mixing of the two aerosols. The mixing was fairly complete as illustrated in Fig. 13, which contains the results for the U_3O_8 aerosol component from three of the four in-vessel filter samplers; sampler 152 did not operate satisfactorily after the first sample was taken.

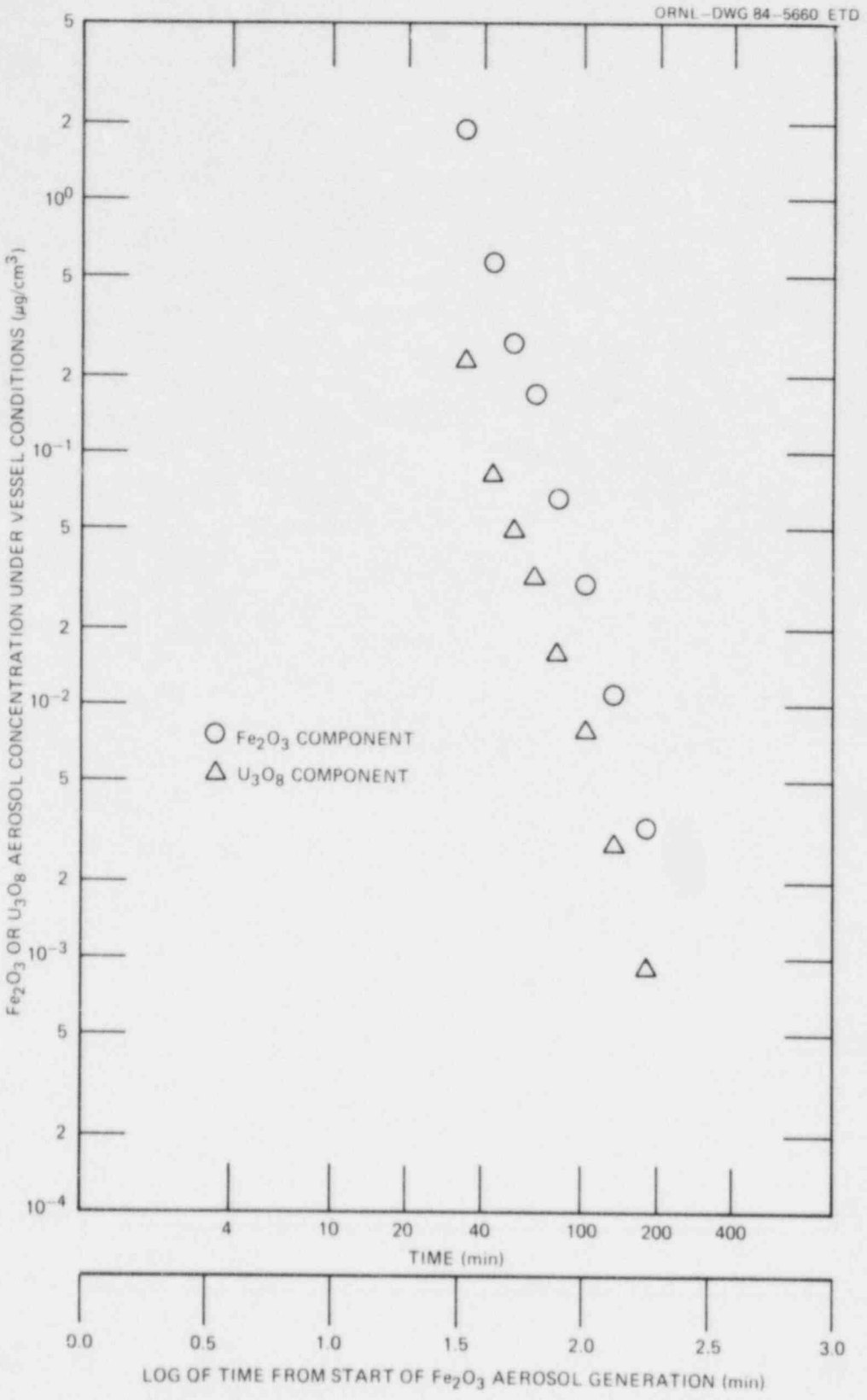

Fig. 12. Average aerosol mass concentrations as function of time for Fe_2O_3 and U_3O_8 components of mixed aerosol in a steam environment (NSPP No. 613).

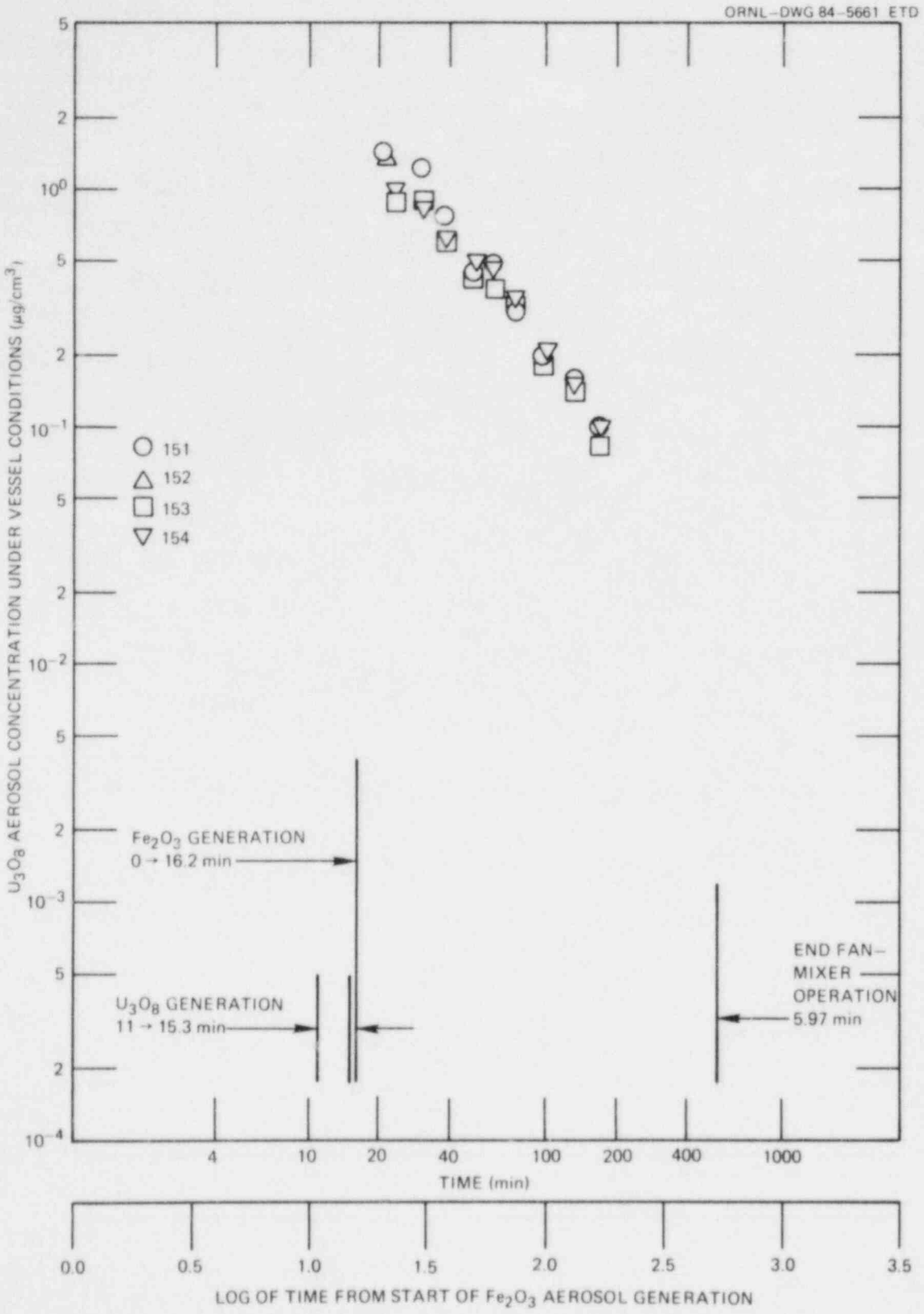

Fig. 13. Aerosol concentration (U_3O_8) as function of time in dry air (RH < 20%) environment (NSPP No. 631).

The first set of aerosol mass concentration samples was taken at 22.3 min (~6 min after termination of Fe_2O_3 aerosol generation). At this time, the average mass concentrations of Fe_2O_3 and U_3O_8 were 0.87 and 1.17 $\mu g/cm^3$, respectively. Extrapolation of these data to the time of Fe_2O_3 aerosol generator cutoff (16.2 min) yields values of 1.2 and 1.7 $\mu g/cm^3$ for Fe_2O_3 and U_3O_8 aerosol, respectively. The rate of disappearance of the two aerosols from the vessel environment is approximately the same as illustrated in Fig. 14; this behavior supports the assumption that the two aerosols are coagglomerated.

Aerosol particle size. The aerodynamic mass median diameter (AMMD) of the aerosol was measured by both the spiral centrifuge sampler and the cascade impactor (Andersen Mark III). Although the vessel did not contain steam, sampling procedures identical to those used in steam, were followed. Six samples as a function of elapsed time were taken for size analysis: four were taken from the auxiliary sampling tank external to the NSPP vessel, and two were taken inside the NSPP vessel. Table 17 contains the results from these samples; determination of the AMMD was made in three ways, one using the U_3O_8 fractional mass, one using the

Table 17. Results from aerosol sizing samples (NSPP No. 631)

Time (min)	Sampler	Location[a]	Aerosol component	AMMD (μm)	σ_g
19.6	Impactor	External	U_3O_8	2.1	1.8
			Fe_2O_3	2.3	1.9
			Total	2.2	1.8
26.0	Centrifuge	External	U_3O_8	2.0	1.4
			Fe_2O_3	1.9	1.6
			Total	1.9	1.5
40.2	Impactor	Internal	U_3O_8	1.7	2.4
			Fe_2O_3	2.2	2.3
			Total	1.9	2.4
66.7	Impactor	External	U_3O_8	1.5	2.7
			Fe_2O_3	1.1	2.5
			Total	1.3	2.8
73.5	Centrifuge	External	U_3O_8	3.1	1.6
			Fe_2O_3	2.1	1.7
			Total	2.7	1.7
112	Impactor	Internal	U_3O_8	1.1	2.3
			Fe_2O_3	1.3	2.0
			Total	1.1	2.2

[a]External means sample processed through external dilution tank before introduction into sampler; internal means sampler installed inside vessel.

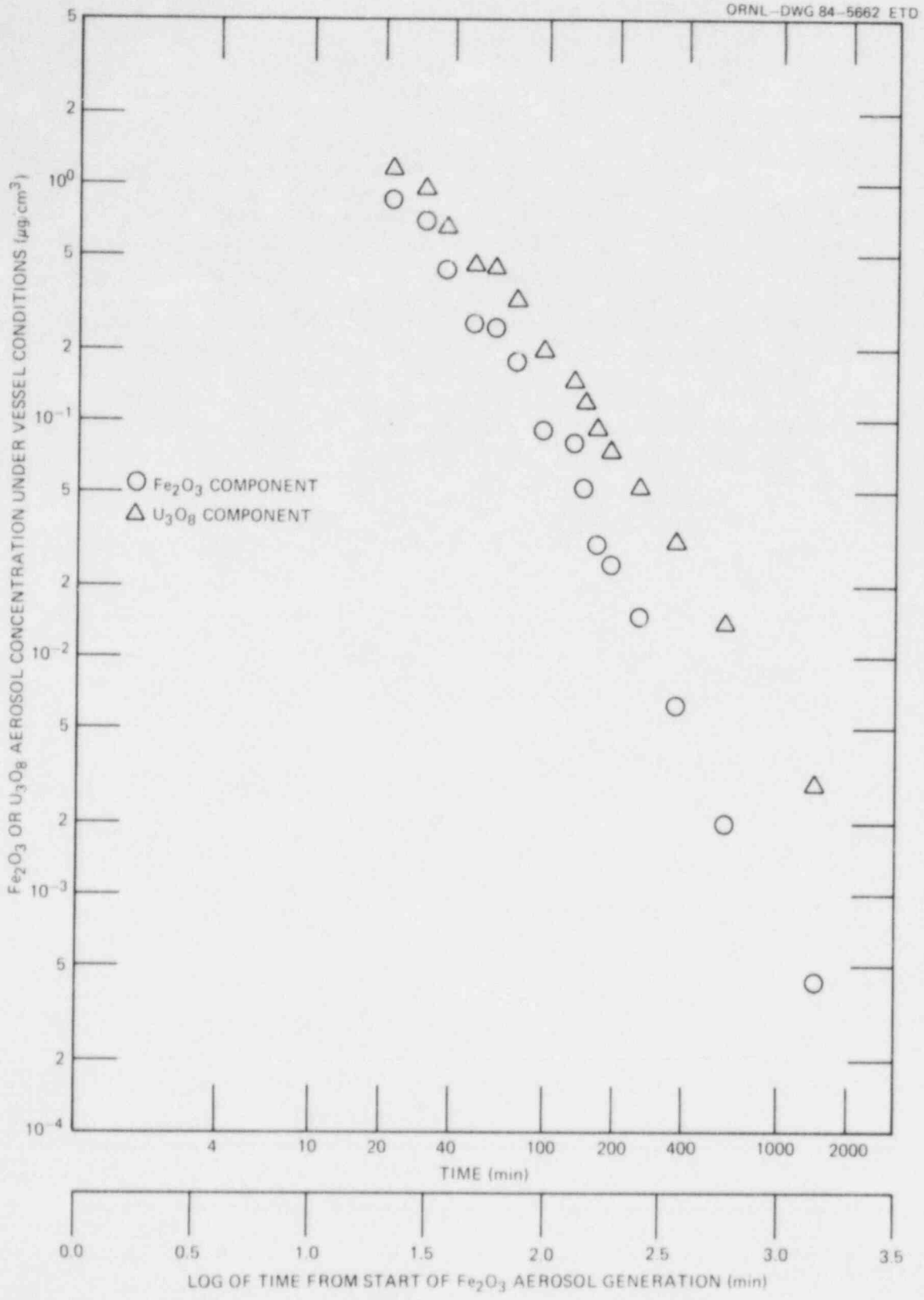

Fig. 14. Average aerosol mass concentrations as function of time for Fe_2O_3 and U_3O_8 components of mixed aerosol in dry air (RH < 20%) environment (NSPP No. 613).

Fe_2O_3 fractional mass, and one using the total aerosol mass, $Fe_2O_3 + U_3O_8$. For the most part, equivalent values were calculated, lending support to the contention that the two aerosols are coagglomerated.

Aerosol distribution. At the termination of the experiment (24 h), the approximate distribution of the mixed aerosol $Fe_2O_3 + U_3O_8$), as determined by the total fallout samplers, the total plateout samplers and the final filter samples was as follows: aerosol settled onto the floor of the vessel, 52%; aerosol plated onto internal surfaces, 48%; and aerosol still suspended in the vessel atmosphere, nil.

2.2.4 Influence of steam environment on behavior of mixed $Fe_2O_3 + U_3O_8$ aerosol

Four mixed aerosol experiments involving various mixtures of Fe_2O_3 and U_3O_8 aerosols have been completed; three were conducted in a steam-air environment and one in a dry air (RH < 20%) environment. A summary of experimental details and results is contained in Table 18.

The behavior of the mixed aerosol ($Fe_2O_3 + U_3O_8$) in a steam-air environment has been similar in the three experiments conducted, although the mass ratio of Fe_2O_3 to U_3O_8 has been varied in each one. The airborne aerosol mass fraction ($Fe_2O_3 + U_3O_8$) airborne (C/C_{max}) as a function of time *after* termination of aerosol generation for these three tests is illustrated in Fig. 15. Although the rate of aerosol removal is somewhat larger for the first 30 min, or so, in Nos. 611 and 613 as compared to No. 612, the time required for 99% removal of aerosol mass from the volume of the vessel is about 60 min in all three experiments. SEM photographs of the mixed aerosol showed almost spherical clumps of aerosol in each case. The AMMD of the mixed aerosol in all cases was in the 1- to 1.7-μm range.

To illustrate the effect of steam on the behavior of the mixed aerosol, the results from experiment 631 are compared with those of Nos. 611–613 in Fig. 16. Under dry air conditions, the mixed aerosol tends to remain airborne longer than under steam-air conditions. Note that the time required for 99% of this aerosol to be removed from the vessel is about 400 min as compared with 60 min for the aerosol in the steam-air environment. SEM photographs show the aerosol to be in the form of chain-agglomerates (as noted in previous experiments with Fe_2O_3 or U_3O_8 aerosol in dry air) rather than in spherical clumps as in Nos. 611–613. The AMMD for the mixed aerosol is slightly larger in the dry atmosphere with a value as large as 2.7 μm being observed.

2.3 Basic Aerosol Experiments

G. W. Parker A. L. Sutton, Jr.
G. E. Creek (Consultant)

The basic aerosol experimental program has been temporarily redirected to provide technical support in various aspects of aerosol generation to the LWR primary-system aerosol transport test (ATT) program at

Table 18. Summary of NSPP experimental details and results

Experiment No.	Vessel atmosphere	Total aerosol generation period (min)	C_{max}[a] $Fe_2O_3 + U_3O_8$ ($\mu g/cm^3$)	Mass ratio Fe_2O_3/U_3O_8	Total fallout (%)	Total plateout (%)	AMMD[b] range (μm)
611	Steam-air	11.5	9.5	1.4/1	83	17	1.0–1.7
612	Steam-air	25.5	2.3	0.3/1	76	24	1.5
613	Steam-air	26.0	7.5	9.7/1	65	35	1.0–1.7
631	Dry air	16.2	2.9	0.7/1	52	48	1.1–2.7

[a]Value obtained by extrapolating data to time of generator cutoff.

[b]Aerodynamic mass median diameter; range of values measured during experiment; total aerosol ($Fe_2O_3 + U_3O_8$).

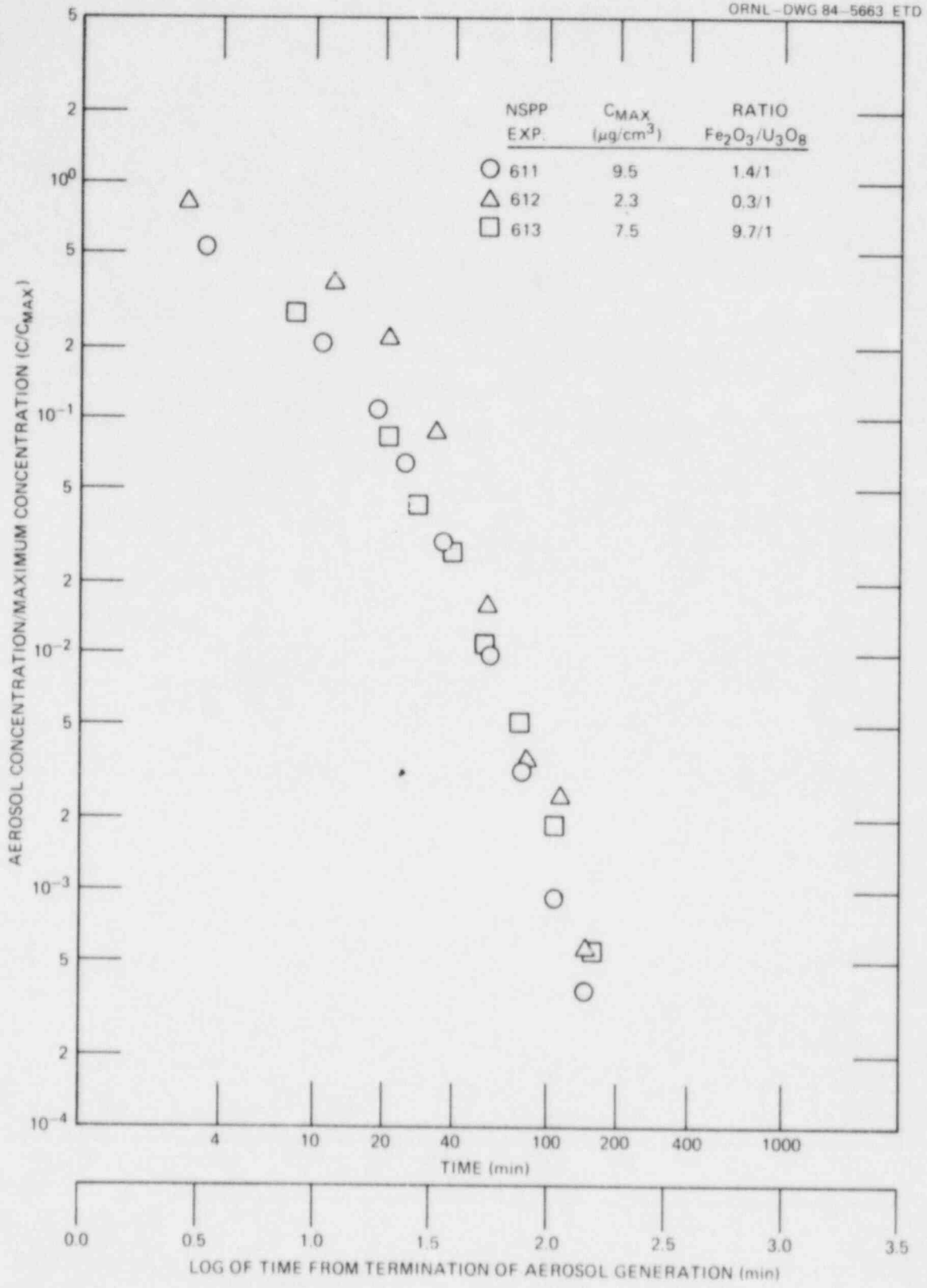

Fig. 15. Comparison of behavior of mixed aerosols (Fe_2O_3 + U_3O_8) in steam-air environment (NSPP Nos. 611–613).

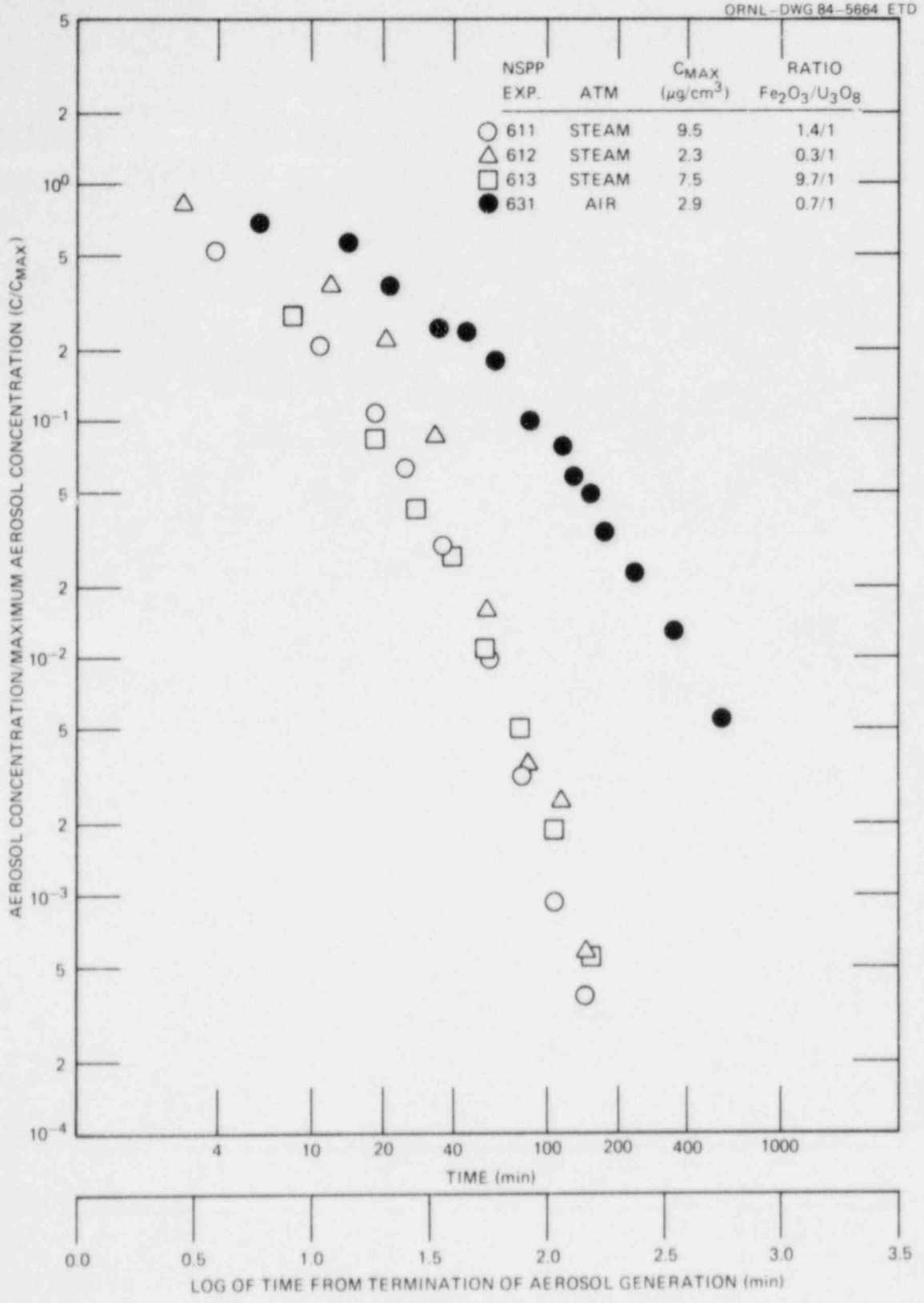

Fig. 16. Comparison of behavior of mixed aerosols (Fe_2O_3 + U_3O_8) in steam-air and dry air environments.

the Marviken facility in Sweden and the large-scale test program on LWR aerosol behavior in containment (DEMONA) at the Battelle (Frankfurt, West Germany) facility.

One area of assistance concerns the design and the operation methods of PT generators of the sizes and types needed for these facilities. For the Marviken facility, the generation of aerosols of a "fissium" mixture (CsOH, RuO_2, SrI_2, and metallic Te) is of interest, while the Battelle-Frankfurt program is concerned with methods of generating iron oxide or tin oxide aerosols or an alternate candidate oxide at the maximum rate. Design details, and drawings of the ORNL-developed metal-oxygen dc PT aerosol generator have been furnished to the two projects.

Plans are being made for using the CRI-II facility, which has external heating and temperature control, for a trial test of the aerosol generator under steam atmosphere conditions. Initially, only low-pressure steam of 15 to 30 psi will be applied to determine the extent of impairment of the aerosol generation efficiency. The design limit of the CRI facility is ~75 psi, but this amount of pressure cannot presently be accommodated by the existing powder feeders without placing them in added pressurized containment.

In the area of sampling equipment development, a small Lovelace Aerosol Particle Separator is being refitted to adapt it to the 250-V 50-cycle Swedish electrical power system. In addition, a variable-speed option will be provided to improve the size discrimination range for larger particles.

2.4 Core-Melt ART Project

G. W. Parker A. L. Sutton, Jr.
G. E. Creek (Consultant)

2.4.1 Introduction

The core-melt ART experiments are intended to address phenomena associated with LWR Class IX accidents, particularly the postulated large-scale vaporization and aerosol formation by fission products, core components, and structural materials. To attain the desired high temperature and melting rates, the radio frequency (rf) induction melting of Zircaloy-clad fuel pins in presintered, powdered oxide crucibles of ThO_2 (the skull-melting technique) has been chosen as the basis of the experimental system.

Previous work has dealt with pressurized-water reactor (PWR) silver alloy control rod interaction with Zircaloy cladding and extensive vaporization of cadmium and silver at temperatures as low as 1400°C, the temperature at which the stainless steel sleeve containing the alloy appears to rupture. The cladding is found to be extensively wetted by the silver through formation of low-melting silver-zirconium alloy. Upon further temperature increase, the cladding is melted off the UO_2. The pellets are left in a free-standing mode presenting the appearance of being wetted by a UO_2-Zr solid solution or pseudo-eutectic. Further heating in steam

to ~2400°C produces a liquid phase containing both Zr and ZrO_2, in addition to UO_2. The silver-zirconium phase is not distinguishable in the eutectic mixtures. Free metallic uranium has been reported by others to be formed at the Zr-UO_2 interface, and evidence for this formation has been obtained through our identification of a U-Zr phase in the metallic stainless steel residue.

More recently, the direction of the project has been toward a critical examination of fission-product release fractions and an evaluation of differences in release rates observed on a smaller scale at KfK compared with the larger (1-kg) ORNL experiments. Several contributing factors inherent in the different experimental approaches toward demonstrating core-melt release seem to account for the variances. However, there is no obvious means of resolving the differences, because they appear to be locked in with the unique approach of each of the experimental routines.

2.4.2 LWR core-melt release correlation with MARCH accident sequences

The application of LWR release data from the ORNL 1-kg core-melt experiments to a specific unprotected LMFBR accident was recently attempted in a study by Reynolds et al.[7] (University of Virginia), along with other data.

In reviewing the ORNL core-melt data, Reynolds was able to conclude that the predicted releases from our LWR data were relatively low in comparison with those calculated by a diffusion model related to very small fuel particles following core degradation; however, he further commented that release rate data were not proposed in the various ORNL progress reports from which he had derived his numerical tables.

By way of alleviating Reynold's difficulty, we have proposed a simple core-melt behavior concept based on both MARCH-I and MARCH-II for the PWR AD and ABγ-2 sequences, for which we have proposed both total releases as well as individual fission-product time-dependent release fractions or release rates.

The basic philosophy of this concept is derived from the analysis of the mode of core degradation in the MARCH (BOIL) projection. According to this interpretation, after the initial blowdown and coolant boiloff, heat generated in the core flows from its approximate center both axially and radially. There is a large temperature difference (initially between 2277°C and 250°C) after about 5 to 10 min. As the molten zone expands at a rate of nearly 1 ft/min in diameter, the temperature rises and becomes more uniform and a 50% volume decrease is effected by collapse of the upper portions of the fuel rods into the melt zone.

In succession, both radial and axial increments of the core are added to the melt zone so quickly that both the portion of the fuel melting and the portion of the fission products vaporizing is relatively constant except for the difference attributed to the induced burnup concentration gradient. The time at temperature for the fuel in the peripheral zones passing from a threshold temperature likely to contribute only volatile fission products by secondary processes is so short that the contribution is essentially negligible. Therefore, we have arbitrarily equated the

fraction of the core melted to the fraction of the volatile fission products released, and all other fission-product release fractions are then simply proportional to the fraction melted. The individual release fractions are taken from our 1-kg core-melt summary data[8] and are used as the end point in the release accumulation curves. In the subsequent calculations, these values are designated by R_{cm}.

In the following material we have prepared both tables and graphs from MARCH-II that describe (1) the nature of the fast melt core heat-up, (2) the corresponding cladding oxidation rate, and (3) the material behavior after initial blowdown and up to core collapse (see Table 19 and Fig. 17).

The method of calculating fission-product distribution at the middle of core life for the Surry ABγ-2 sequence is based on MARCH-II, which divides the reactor core into 10 vertical cylinders; each cylinder is in turn divided into 24 units of equal volume. The fraction of the core

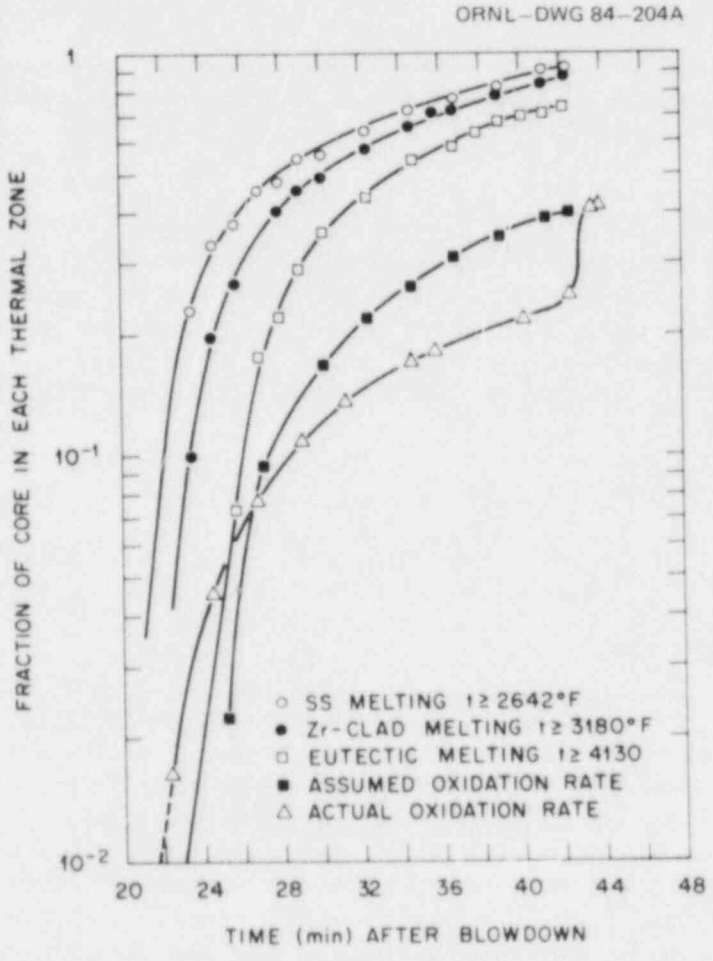

Fig. 17. Reactor accident Surry ABγ-2 sequence.

Table 19. Accumulated release fractions for ABγ-2

Time (min)	Fission element control material or structural component									
	I, Cs	Mo	Sr	Ba	Sn	Mn	Ag	In	Cd	Fe
25.6	0.073	1.02E-4	5.7E-3	4.8E-3	8.8E-4	8.8E-3	4.50E-3	0.40E-3	0.039	5.9E-5
26.7	0.175	2.50E-4	1.4E-2	1.2E-2	2.1E-3	2.1E-2	1.07E-2	9.50E-3	0.093	1.4E-4
27.8	0.218	3.1E-4	1.7E-2	1.4E-2	2.6E-3	2.6E-2	1.33E-2	1.20E-2	0.116	1.7E-4
28.9	0.287	4.0E-4	2.2E-2	0.019	3.4E-3	3.4E-2	1.75E-2	1.55E-2	0.150	2.3E-4
30.0	0.362	5.1E-4	2.8E-2	0.024	4.3E-3	4.3E-2	0.022	1.96E-2	0.192	2.9E-4
32.2	0.440	6.1E-4	3.4E-2	0.029	5.3E-3	5.3E-2	0.038	2.42E-2	0.230	3.5E-4
34.4	0.540	7.5E-4	4.2E-2	0.035	6.4E-3	6.4E-2	0.033	2.90E-2	0.280	4.3E-4
36.6	0.590	8.2E-4	4.6E-2	0.039	7.0E-3	7.0E-2	0.036	3.20E-2	0.310	4.7E-4
37.7	0.640	9.0E-4	5.0E-2	0.042	7.7E-3	7.7E-2	0.039	0.04E-2	0.340	5.1E-4
38.8	0.670	9.3E-4	5.2E-2	0.044	8.0E-3	8.0E-2	0.041	3.60E-2	0.350	5.3E-4
39.9	0.700	9.8E-4	5.4E-2	0.046	8.4E-3	8.4E-2	0.042	3.80E-2	0.370	5.6E-4
41.0	0.710	1.0E-3	5.6E-2	0.047	8.6E-3	8.6E-2	0.043	3.85E-2	0.380	5.7E-4
42.1	0.740	1.0E-3	5.8E-2	0.049	8.9E-3	8.9E-2	0.045	4.00E-2	0.390	5.9E-4

volume represented in each of these hypothetical cylinders is:

$$V_1 = 0.047 \qquad V_6 = 0.062$$
$$V_2 = 0.062 \qquad V_7 = 0.083$$
$$V_3 = 0.083 \qquad V_8 = 0.124$$
$$V_4 = 0.062 \qquad V_9 = 0.166$$
$$V_5 = 0.062 \qquad V_{10} = 0.249$$

It is estimated that one-half of the fission-product inventory of the reactor is contained in V_1–V_5; one-third is contained in V_6, V_7 and V_8; and one-sixth is contained in V_9 and V_{10}. The reactor inventory is thus divided horizontally into sixths.

Each of the above sections (vertical) is divided into 24 units of equal volume. N_1, N_2, N_3,...N_{10} is the number of units in V_1, V_2, V_3... V_{10} that are molten [temperature 2277°C (4130°F)] at any time.

The fractional accumulated release by time interval R_t is calculated from the following expression:

$$R_t = \left[\frac{3}{5} \sum_{i=1}^{5} N_i + \frac{2}{3} \sum_{i=6}^{8} N_i + \frac{1}{2} \sum_{i=9}^{10} N_i \right] R_{cm}/(6 \times 24) \ . \qquad (1)$$

Results of these calculations are given in Table 19 and Fig. 18.

The accumulated release curves shown in Fig. 18 can be adequately represented by an equation of the form:

$$F = (AT - C)/(1 - BT) \ , \qquad (2)$$

where

F = fraction released,
T = time (min) from 25.6 to 42.1 min.

A, B, C are constants that define the individual release curves. Values for the constants A, B, and C are listed in Table 20.

2.4.3 Release rates calculated from accumulated release totals

While it would be possible to derive some release rate data from our 1-kg core-melt experiments, which were generally conducted in steps of successively higher temperature, our opinion is that this would serve no useful purpose because it does not reflect the actual reactor course of events in which melting is continuous. Instead, the release rates (fraction of reactor release per minute) can be computed from the differentiation of Eq.(2) that gives:

$$F' = (A - BC)/(1 - BT)^2 \ . \qquad (3)$$

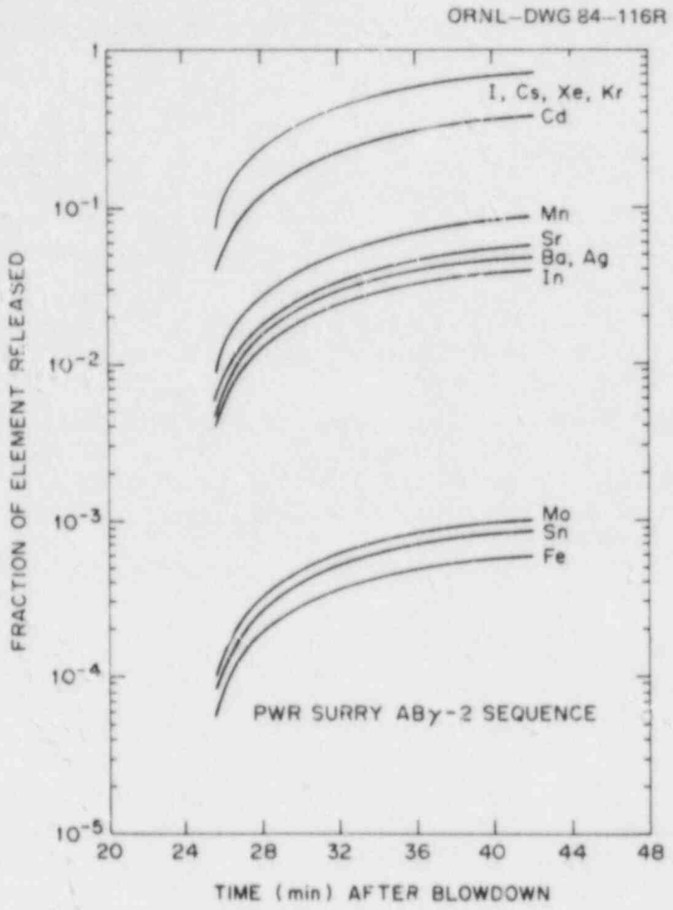

Fig. 18. Accumulated release fraction (R_{cm}) for core-melt.

Table 20. Values for the constants in Eq. (2)

Element	Constant		
	A	B	C
Cs, I	−1.40E-1	1.022E-1	−3.492
Mo	−1.35E-4	7.9E-2	−3.348E-3
Sr	−1.255E-2	1.13E-1	−3.105E-1
Ba	−1.41E-2	1.427E-1	−3.482E-1
Sn	−2.217E-3	1.266E-1	−5.478E-2
Mn	−2.217E-2	1.266E-1	−5.478E-1
Ag	−6.859E-3	8.712E-2	−1.701E-1
In	−8.501E-3	1.114E-1	−2.103E-1
Cd	−1.016E-1	1.315E-1	−2.508
Fe	−1.157E-4	1.046E-1	−2.862E-3
B	−1.799E-3	1.227E-1	−4.45E-2

The release rate (fraction/min) for each species is listed in Table 21 and compared in Fig. 19.

2.4.4 Volatility of boric oxide in a core-melt environment

The first BWR type control rod interaction and vaporization test (CM-37) was conducted using an array of three B_4C powder-filled stainless steel tubes with the amount of B_4C in the ratio of 1:100 to the amount of UO_2. The sealed tubes were placed between the Zircaloy-clad UO_2 pellets in the usual configuration. At a temperature above 1500°C, the release of a white aerosol (assumed to be B_2O_3) was continuously observed but appeared to diminish in rate at the highest temperature, 2400°C. Only about 1.03% of the added B_4C was actually released as B_2O_3; however, there is a possibility of solid solution with UO_2.

The ceramics phase diagram handbooks do not contain a reference to a UO_2–B_2O_3 or ZrO_2–B_2O_3 system having been studied. The analogous ThO_2–B_2O_3 system, which is published, does show liquid phases above 1500°C.

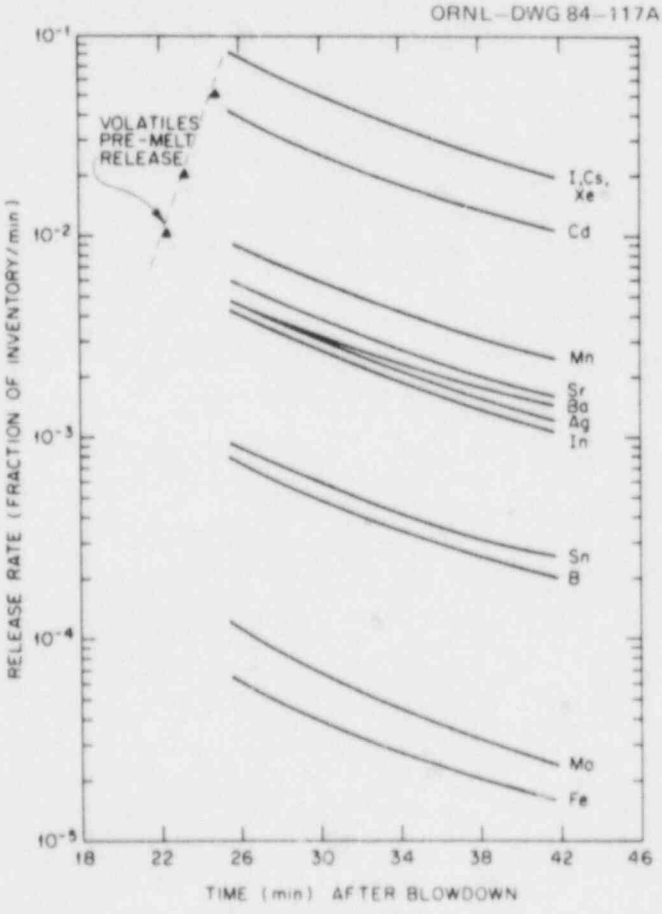

Fig. 19. Rate of aerosol release for AB sequence.

Table 21. Aerosol release rate for core-melt ABγ-2 accident sequence

Time (min)	Fraction released per minute										
	Cs, I	Mo	Sr	Ba	Sn	Mn	Ag	In	Cd	Fe	B
25	8.6E-2	1.2E-4	6.7E-3	5.7E-3	1.04E-3	1.0E-2	5.3E-3	4.7E-3	4.6E-2	6.9E-5	8.6E-4
26	7.7E-2	1.1E-4	6.0E-3	5.1E-3	9.20E-4	9.2E-3	4.7E-3	4.1E-3	4.1E-2	6.1E-5	7.7E-4
28	6.1E-2	8.6E-4	4.8E-3	4.1E-3	7.40E-4	7.4E-3	3.7E-3	3.3E-3	3.3E-2	4.9E-5	6.1E-4
30	5.0E-2	7.05E-5	3.9E-3	3.3E-3	6.00E-4	6.0E-3	3.1E-3	2.7E-3	2.7E-2	4.0E-5	5.0E-4
32	4.2E-2	5.90E-5	3.3E-3	2.8E-3	5.00E-4	5.0E-3	2.6E-3	2.3E-3	2.2E-2	3.4E-5	4.2E-4
34	3.6E-2	5.00E-5	2.8E-3	2.3E-3	4.30E-4	4.3E-3	2.2E-3	1.9E-3	1.9E-2	2.8E-5	3.4E-4
36	3.1E-2	4.30E-5	2.3E-3	2.0E-3	3.70E-4	3.7E-3	1.9E-3	1.6E-3	1.6E-2	2.4E-5	3.1E-4
38	2.6E-2	3.70E-5	2.1E-3	1.7E-3	3.20E-4	3.2E-3	1.6E-3	1.4E-3	1.4E-2	2.1E-5	2.6E-4
40	2.3E-2	3.20E-5	1.8E-3	1.5E-3	2.80E-4	2.8E-3	1.4E-3	1.3E-3	1.2E-2	1.9E-5	2.3E-4
42	2.0E-2	2.90E-5	1.6E-3	1.4E-3	2.50E-4	2.5E-3	1.3E-3	1.1E-3	1.1E-2	1.6E-5	2.0E-4
43	1.9E-2	2.70E-5	1.5E-3	1.3E-3	2.30E-4	2.3E-3	1.2E-3	1.0E-3	1.0E-2	1.5E-5	1.9E-4

This gives us reason to suspect that similar solid solutions for ZrO_2–UO_2–B_2O_3 should exist. To explore this effect specifically, we next conducted a melt test with B_2O_3 powder intimately mixed with UO_2 powder and melted completely in the regular fuel assembly in steam. This was done in experiment CM-38, and the total B_2O_3 (Table 22) release was measured at only 0.45% or about one-half of that measured in the B_4C oxidation test in CM-37 above. Continuing in this investigation, the volitility of B_2O_3 from the ZrO_2-B_2O_3 mixture (CM-39) was also measured. This gave an almost identical release (0.93%) as volatile B_2O_3.

Table 22. Summary of boron release experiments

Run No.	Total boron (g)	Heat A (1600°C)		Heat B (1800°C)		Heat A and B	Heat C (2400°)		Total release from A, B, C (%)
		Filter (%)	Wash (%)	Filter (%)	Wash (%)	Wash (%)	Filter (%)	Wash (%)	
CM-37	2.55[a]	0.093	0.15	0.23	0.14	0.29	0.064	0.043	0.72
CM-38	0.66[b]	0.056		0.28		0.03	0.13	0.003	0.5
CM-39	0.40[c]	0.015	0.88	*d*	*d*	*d*	0.008	0.025	0.93

[a]Present as B_4C.

[b]Present as B_2O_3-UO_2 mixture.

[c]Present as B_2O_3-ZrO_2 mixture.

[d]Analysis of B and C heats combined.

Since the possibility remains that under some accident scenarios, borated water may be injected in the core prior to meltdown, we next conducted an experiment in which the water used in the steam generation process was mixed with soluble boron or sodium pentaborate to about the maximum 2000-ppm level usually provided in the reactor. This final boric oxide test (CM-40) was performed by adding boric acid (+NaOH) to the feedwater used to generate steam, much the same as is expected to occur in the reactor with the injection of emergency core coolant water. In this case, we found that during the lower temperature heating steps (1400 to 1800°C) ~10% of the boron as boric oxide was vaporized, but as the temperature increased to partial melting the release essentially terminated (0.1%), indicating increased reactivity of boric oxide with the hot mixed oxides in the fuel. See Table 23 for details.

The interest in B_2O_3 release, which may occur in case of a severe accident in both types of LWRs, concerns the possible reaction with CsI leading to the formation of volatile HI. If the interaction of B_2O_3 with $ZrO_2 \cdot UO_2$ tends to minimize the release, the CsI reaction could become less significant.

2.4.5 Initial operation of the new 250-kW induction generator

Successful operation of the 250-kW rf induction furnace was demonstrated by heating a simulated large fuel bundle (126 empty, stainless

Table 23. Results of experiment CM-40 on the volatility of boric acid added as emergency control coolant

Heating	Total[a] boron present (g)	Boron released as B_2O_3	
		Filter (%)	Wash (%)
A (1600°C)	0.034	10.37	
B (1800°C)	0.088	5.5	0.68[b]
C (2400°C)	0.142	0.024	0.009

[a]As boric acid in water used for steam generation.

[b]Combined A and B washes.

steel tubes, 12 in. in length and weighing a total of 14.2 kg) to almost melting (~1450°C) in 30 s at the currently available full power; about 45 s heating time was required at about one-half power.

To obtain optimum efficiency of the induction heating process, it was necessary to remove the stepdown transformer from the transmission system and perform the heating with high dc voltage on the load coil. Since no difficulty in the operation was encountered, the decision has been made to accept the high load coil voltage in return for the improved heating efficiency. In terms of real output in rf wattage, we obtained ~150 kW (amperes × plate voltage) with a restricted line breaker limit of 400-A input. With additional main line supply cables, the input to the system could be increased to about 600 A.

A measure of the actual power delivered to the crucible can be made by using it as a calorimeter and calculating total heat removal at equilibrium from the temperature rise of the cooling water. This will be done routinely for each meltdown experiment.

Completing the installation of the safety pressure containment and fitting the quartz chimney (Fig. 20) to the elevating device (Fig. 21) are the principal remaining projects.

Additional photographs are included in this section that show the relative size of the 1- and 10-kg fuel bundles in Figs. 22 and 23.

The rf generator and the parallel transmission lines are shown in Figs. 24 and 25. The test bundle of 126 stainless steel tubes mentioned previously is shown in Fig. 26 at an elevated temperature.

2.4.6 Fuel and control rod procurement

High-density UO_2 fuel pellets in large quantity, preferably depleted in ^{235}U, will be required to conduct the series of 10-kg fuel melt experiments. In the past, we have been able to obtain small quantities of low-grade UO_2 pellets from various fuel recycle demonstration projects at no

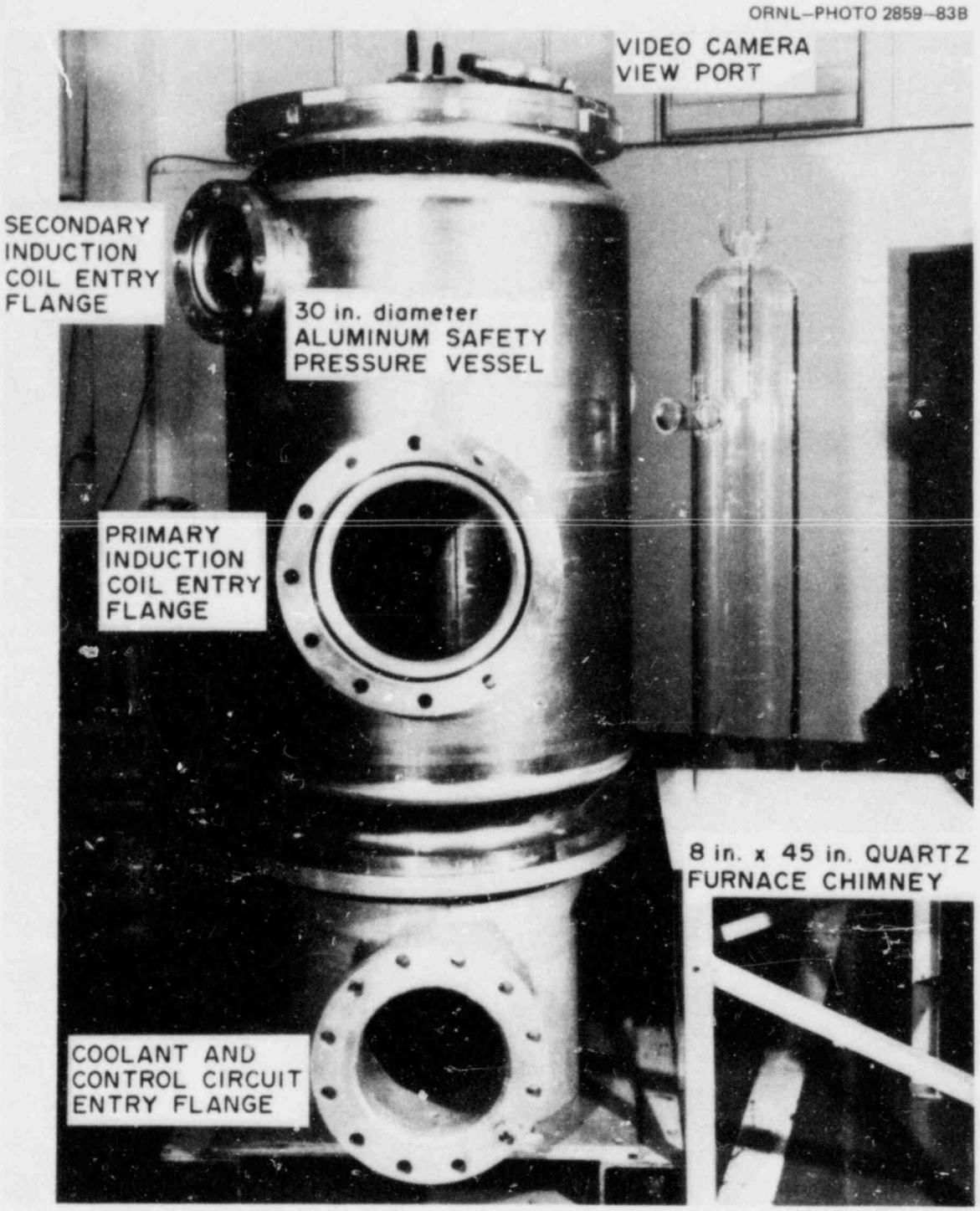

Fig. 20. Housing and furnace for 10-kg fuel melting system.

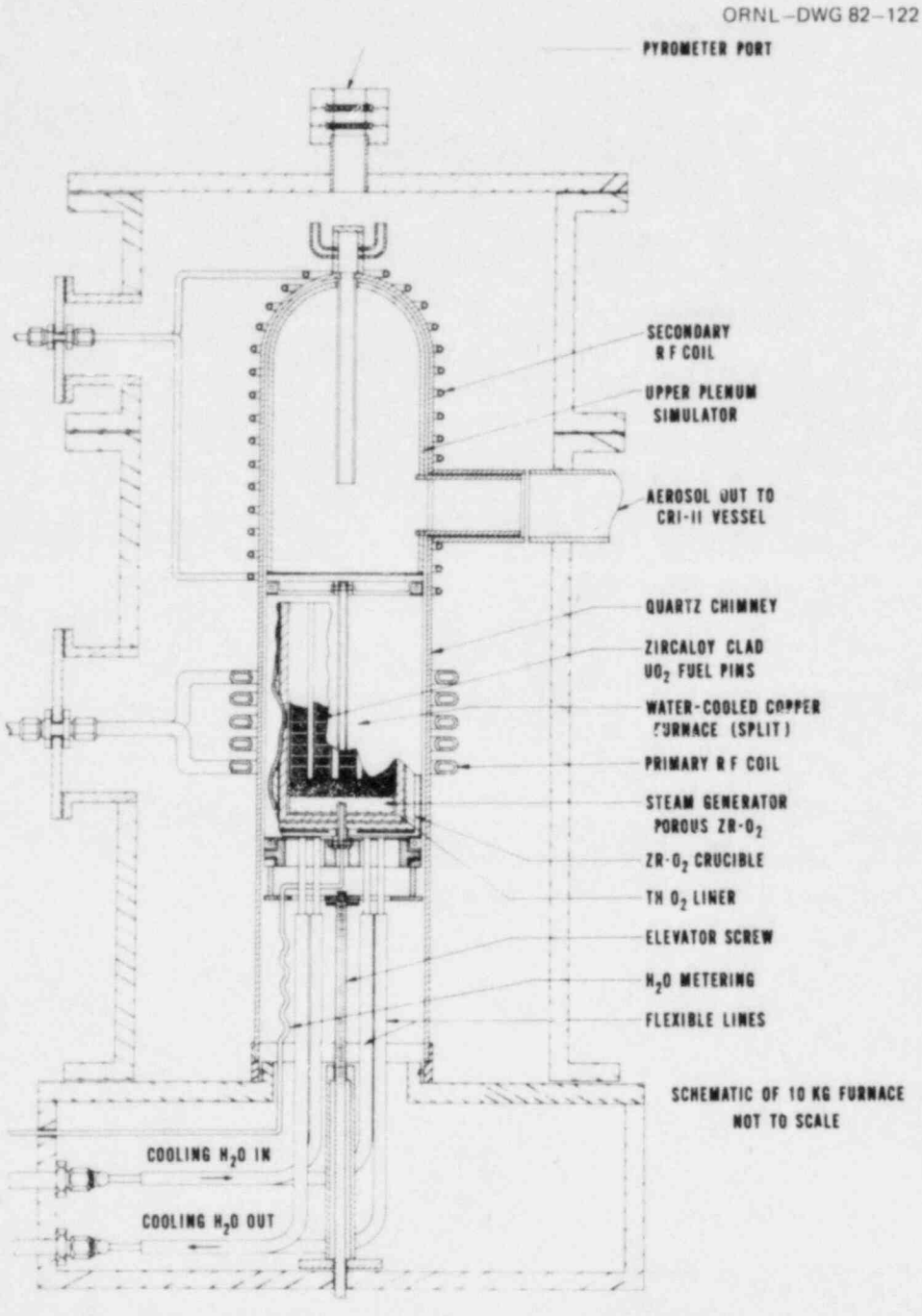

Fig. 21. Design of large induction furnace with elevating jack.

ORNL–PHOTO 5387–83

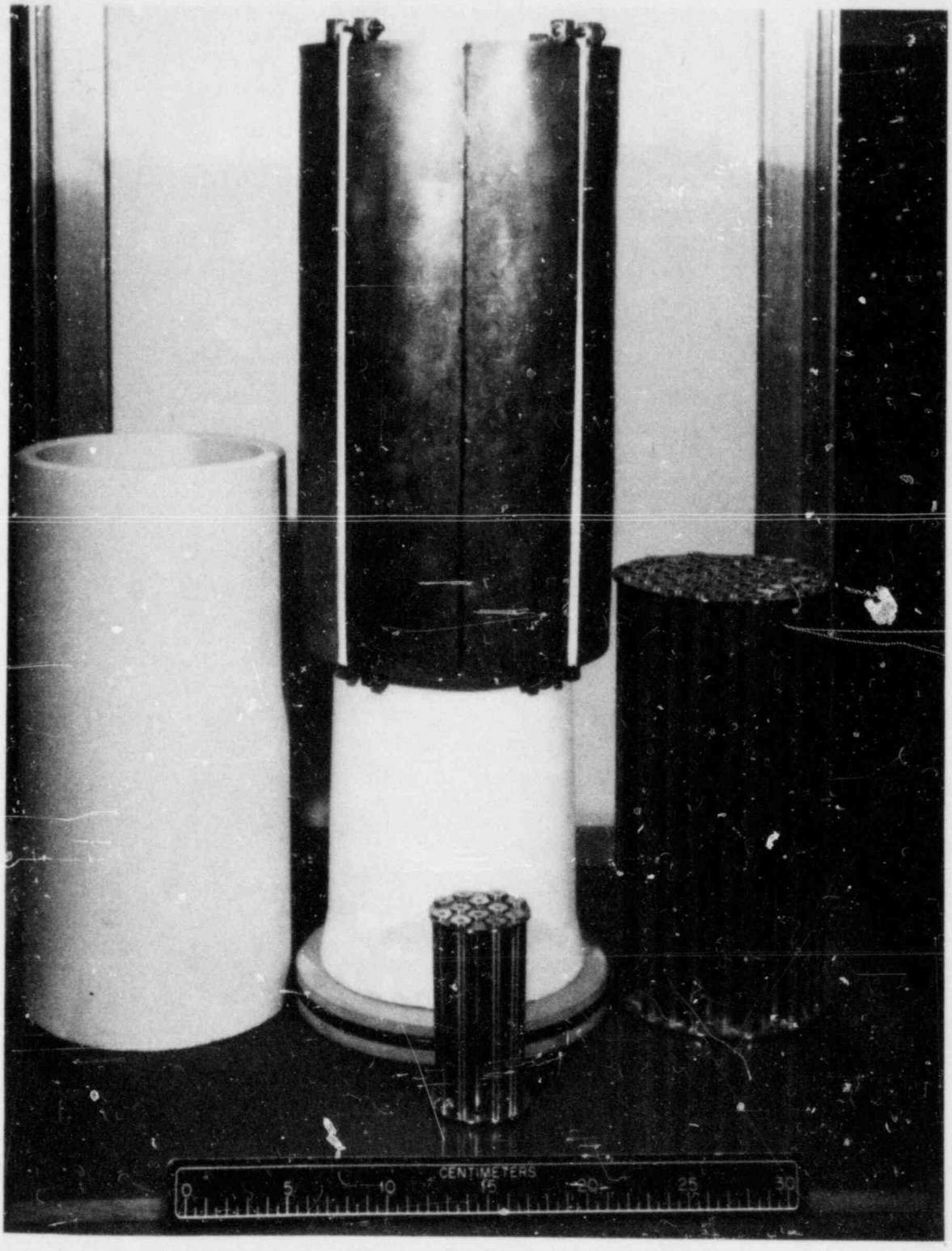

Fig. 22. Comparative sizes of 1-kg and 10-kg fuel bundles.

ORNL-PHOTO 3686-83

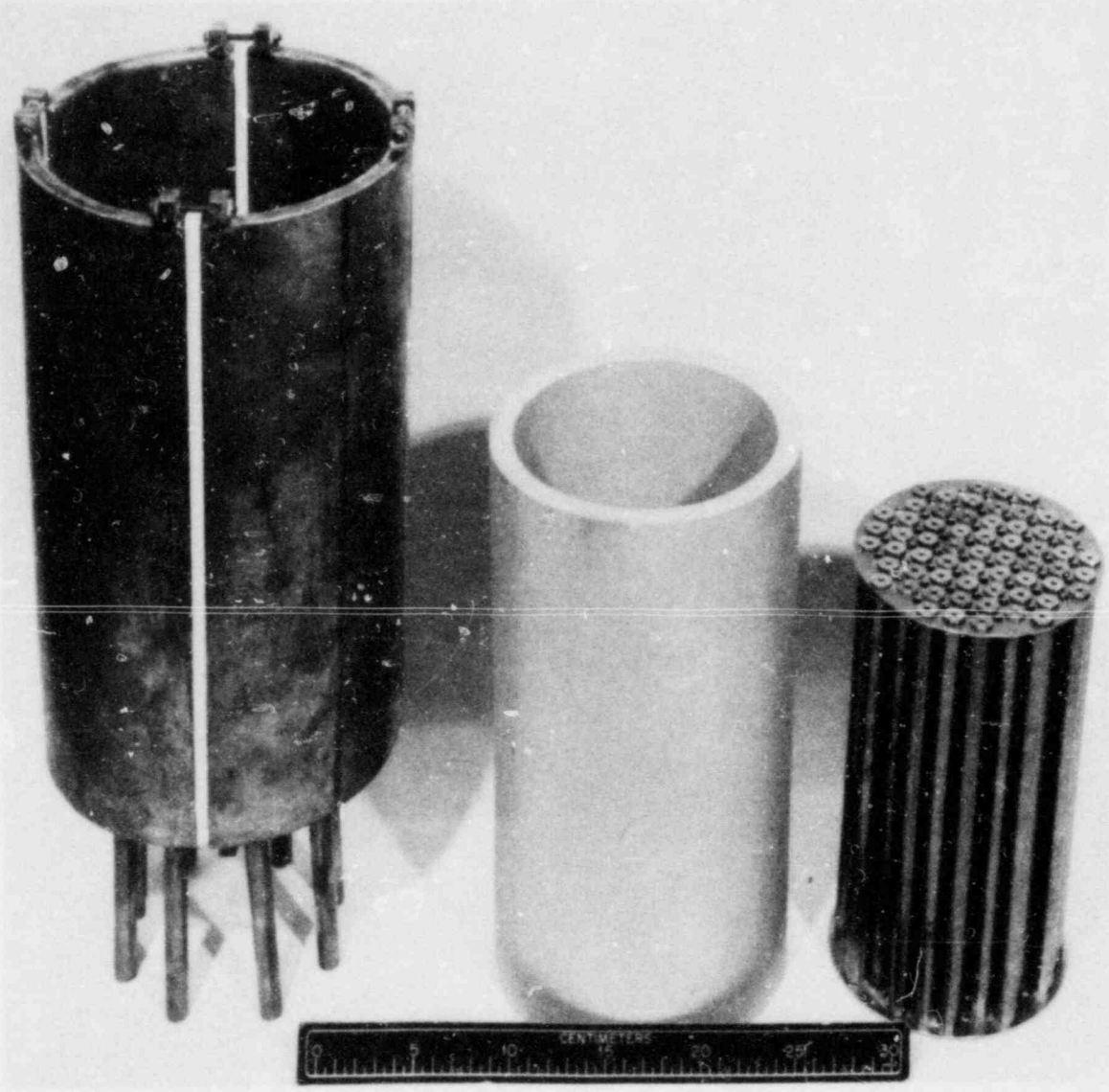

Fig. 23. The 10-kg core-melt components and 62-rod fuel bundle.

cost. For the proposed large-scale operation, we have taken steps to procure about 100 kg of PWR-size pellets that should allow experimental operations for about 1 year.

The silver alloy control rod material requirements will be about 0.25 kg per experiment; this material will be in the form of 5-mm rods about 22 cm in length. The rods will be clad in closely fitted stainless steel and then enclosed in a loosely fitted zircaloy sleeve or guide tube equivalent. Fabrication of about 2.5 kg of the control rod alloy and the necessary sleeve materials has been initiated in the M&C Division of ORNL.

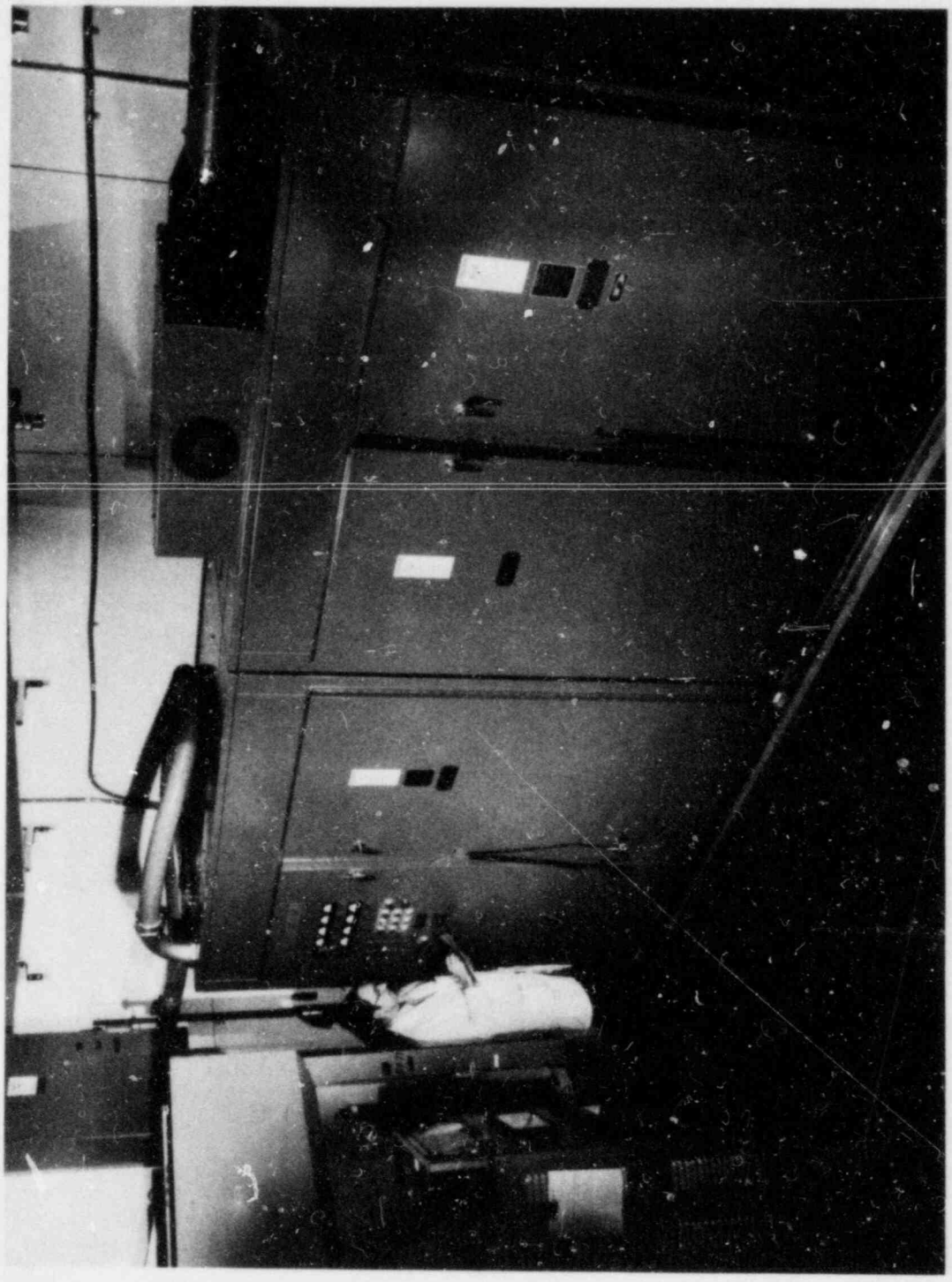

ORNL—PHOTO 0339—84

Fig. 24. New 250-kW induction generator of ORNL.

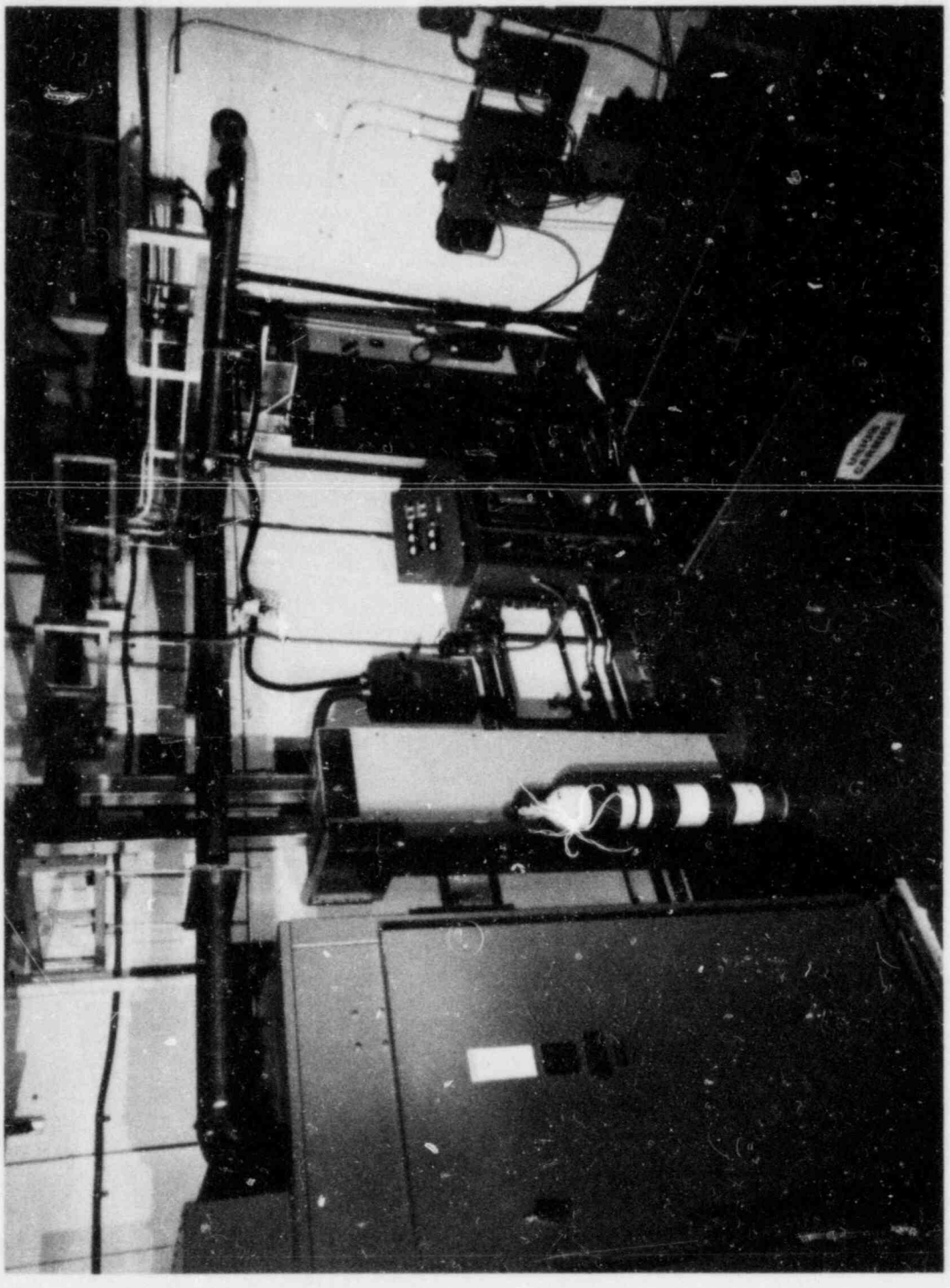

Fig. 25. Induction generator and transmission and cooling system.

ORNL-PHOTO 1520-84

Fig. 26. Initial test of mock-up bundle at elevated temperature.

2.4.7 Program plan

While the original concept of the 10-kg fuel-melt project was intended to emphasize aerosol chemistry and aerosol behavior in the CRI-II containment vessel, recent directions from the project sponsor indicate that the initial experiments should be a scale comparison against the observed fuel-melt behavior and fission element release data obtained from the 1-kg fuel-melt experiments over the last 2 years. Some equipment design changes to implement this alternative objective are currently under consideration.

As a result of this redirection and increased scope of operation, the project is being separated from B0121 and will become a part of B0127, Fission Product Release at Severe Accident Conditions.

3. ANALYTICAL PROGRAM

M. L. Tobias

3.1 Introduction

The analytical efforts in the ART Program consist mainly of mathematical and computational activities designed to process and interpret the data obtained in various experiments. Typical activities in the past have been the development of theories of bubble behavior in the FAST experiment, processing of data from NSPP runs, comparison of predicted aerosol behavior by codes such as HAARM-3 with experiments, implementation of advanced aerosol and bubble behavior codes from various institutions, and the development of models to describe steam behavior in the NSPP.

3.2 Comparison of NAUA Code Predictions with NSPP Aerosol Experiments in Steam-Air Atmospheres

The NAUA code[9] has been used to model some of the experiments in the NSPP steam-air atmospheres. The experiments have been selected from the 400-series[3,10-12] (uranium oxide) and the 500-series[2,3,13] (iron oxide). Tables 24 and 25 list the aerosol generation times and maximum suspended concentrations achieved, as well as the range of dried particle sizes, fraction settled, and steam temperature.

Table 24. NSPP steam-uranium oxide aerosol experiments[a]

Experiment No.	Aerosol generation time (min)	Maximum suspended concentration (g/m^3)
401	10.0	26.0
402	6.5	5.5
403	18.0	9.4
404	16.3	23.0
406	9.0	15.2

[a]Fraction settled 61 to 81%
Dried particle sizes 1 to 2 μm
Steam temperatures 364 to 393 K

Table 25. NSPP steam-iron oxide aerosol experiments[a]

Experiment No.	Aerosol generation time (min)	Maximum suspended concentration (g/m^3)
501	14.0	1.0
502	17.0	1.9
503	25.0	3.7
504	13.5	7.5

[a]Fraction settled 47 to 94%
Dried particle sizes 1 to 2 μm
Steam temperature 381 to 394 K

3.2.1 Effect of diffusional boundary layer thickness

The maximum suspended aerosol concentration reached in experiment 501 was 1 g/m^3, which is at the low end of the concentration level of the 500-series. In Fig. 27, the experimental measurements show an initial bowlike variation up to about 200 min, after which the concentration falls off at a slower rate. This slower rate behavior is characteristic of the experiments, and it is almost impossible to represent it with the HAARM-3 code[14] (Fig. 28). HAARM-3, unlike NAUA, does not include any condensation

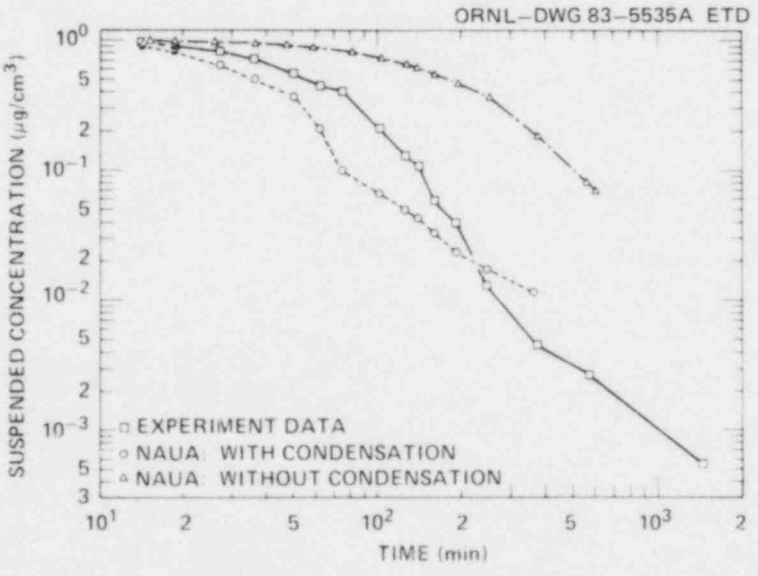

Fig. 27. Experiment 501, iron oxide in steam. Comparison of experimental data with NAUA code results with and without condensation on particles.

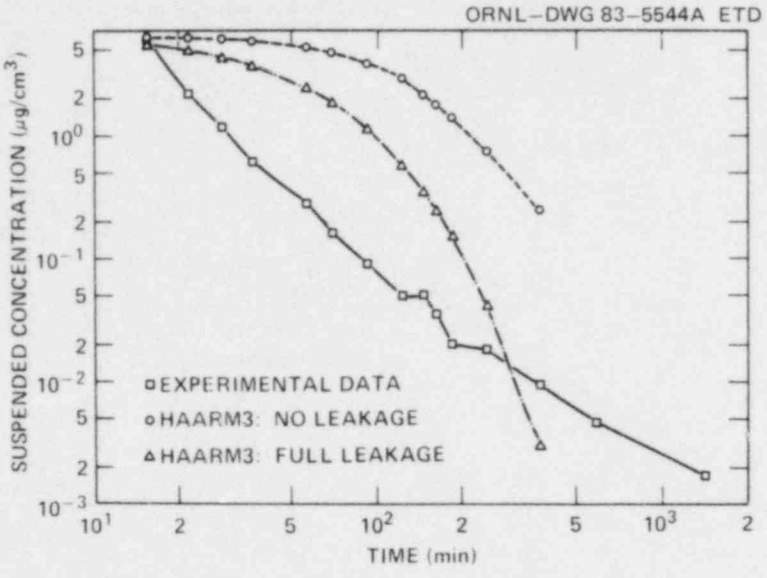

Fig. 28. Comparison of HAARM-3 calculations with iron oxide-steam experiment 504. A leakage rate is assumed for the purpose of simulating diffusiophoretic deposition.

effects. More importantly, it rests on the assumption that the aerosol size distribution is always lognormal. The NAUA code divides the aerosol particle size range into size bins, and the size distribution is determined by the calculation. Figure 27 shows the results of NAUA calculations with and without condensation. If condensation is not assumed to take place, the calculated suspended concentration remains higher than that observed and only falls off when presumably sufficient coagulation has occurred so that faster settling will take place. The case where condensation is assumed shows an initially faster decline in suspended concentration than the experiment, followed by a slower decline at about 70 min. This slowdown may be caused by the larger suspended particles being "washed out" by rapid condensation; if the population is skewed to smaller sizes, condensation will be slowed and settling velocities will be slower than before. This pattern is much like that shown by the experiment, but further examination of the results will be needed to verify these explanations.

In the high concentration case, experiment 504, the suspended concentration reached a maximum of 7.5 g/m^3. In Fig. 29, the suspended concentration variation shows no initial bowing, while all the calculated curves do. Figure 29 also shows the effects of trying to match the observed variation by increasing the rate of diffusional deposition in the calculations. This was done by decreasing the input parameter DELD, the diffusional boundary layer thickness, from 0.01 to 10^{-5} cm. (The value of 0.01 was used for the calculation shown in Fig. 27 and is the value suggested in Ref. 9). This is apparently insufficient to match the observations, mainly because of the "break" that appears in the calculated curves that is suspected to be caused by condensation washout of larger sized particles. Of course, when the value of DELD becomes as low as

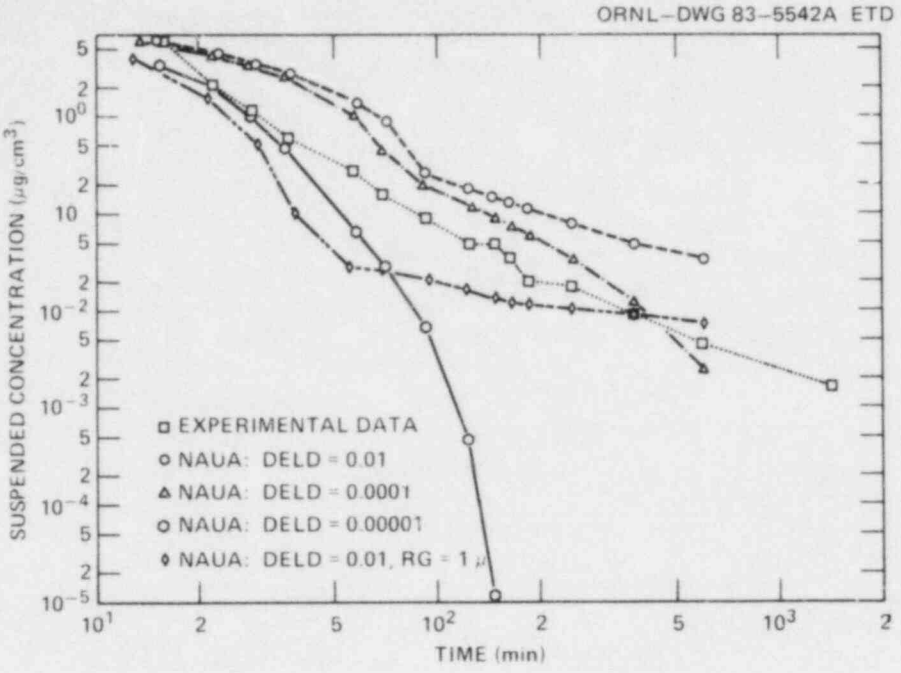

Fig. 29. Experiment 504, iron oxide in steam. Comparison of experimental results with NAUA calculations at various assumed values of diffusional boundary layer thickness and for the separate effect of increasing initial particle size from 0.1 to 1 μm.

10^{-5} cm, the diffusional deposition becomes sufficiently great to mask the presence of other processes, and the suspended concentration falls off sharply with time as shown.

3.2.2 Effect of assumed initial particle size

The remaining curve shows the effect of changing the assumed geometric mean radius from 0.1 μm, used in all the other calculations, to 1 μm. The larger initial size leads to a sharp falloff in concentration, probably because of comparatively high condensation on larger particles. The rate of decrease after about 50 min is then significantly slowed, with the slope somewhat less than that of the top curve where the initial particle radius was taken as 0.1 μm.

3.2.3 Effect of assumed source rate at an assumed initial radius of 1 μm

To improve the match between the NAUA results at 1-μm initial radius and the experiment, the source rate for the aerosol injection was increased. The aerosol source rate in the experiment is not actually known; only the maximum concentration is inferred from the measurements, and the rate is estimated from it. As Fig. 29 shows, the maximum concentration was not reached for the 1-μm-radius case because removal rates during the aerosol injection period were too high. Figure 30 compares the effect

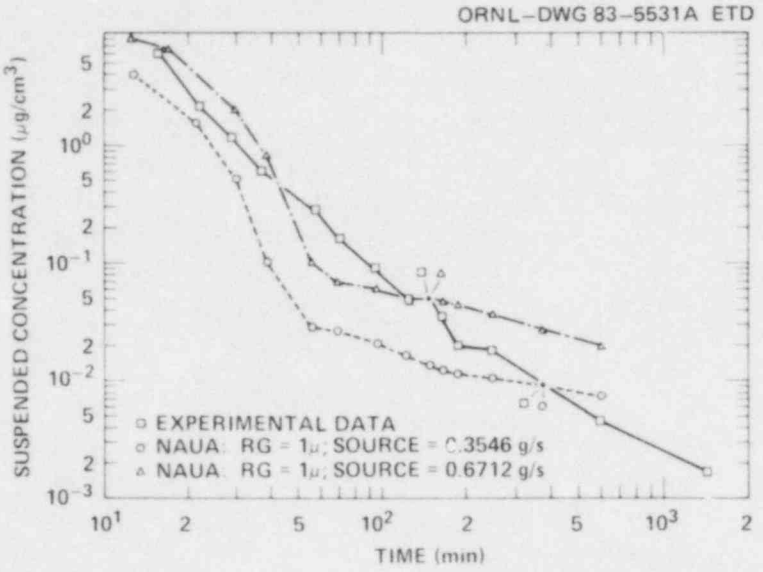

Fig. 30. Experiment 504, iron oxide in steam. Comparison of NAUA calculation at two source rates with experimental data.

of increasing the original rate of 0.3546 g/s to 0.6712 g/s. While the maximum value was matched better, the pattern of concentration decay was no different from that at the lower rate and does not resemble the observed behavior very much.

3.2.4 Diffusiophoretic effects

The NAUA code does not deal with thermophoretic or diffusiophoretic effects. Only a diffusional deposition model is included, that is, a deposition caused by the concentration difference between the containment volume and the wall. Diffusiophoretic deposition can be represented, however, by assuming that a leakage of aerosol exists that is proportional to an assumed condensation rate of steam at the wall of the NSPP vessel. This approach was applied to experiment 401 (uranium oxide in steam). In Fig. 31, the measured suspended concentration is first compared with a calculation involving steam condensation on the aerosol particles. As with iron oxide cases, the slope of the curve becomes less steep after the presumed initial washout; in this case, the concentration "hangs up" at about 75 min. Addition of the leakage process provides a continuous removal mechanism, and the calculated curve follows the experiment better than the curve with condensation only.

The results of this approach were less successful for the iron oxide experiments. Figure 32 shows the results for experiment 501. With a leakage rate (100%) corresponding to a steam injection rate of 10.96 g/s into the NSPP vessel, a concentration-vs-time curve results (the lowest curve on Fig. 32) that falls off too rapidly at first, slows, and then falls off more quickly. This pattern may have to do with an oscillating kind of washout process produced by a changing balance between supersaturation and particle size. Cutting down the leakage rate by one-half

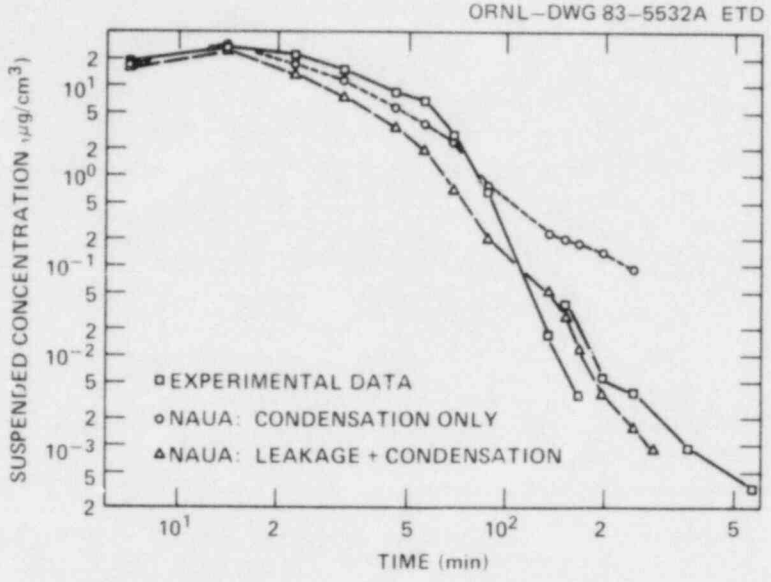

Fig. 31. Experiment 401, uranium oxide in steam. Effect of an assumed leakage rate to represent diffusiopheresis.

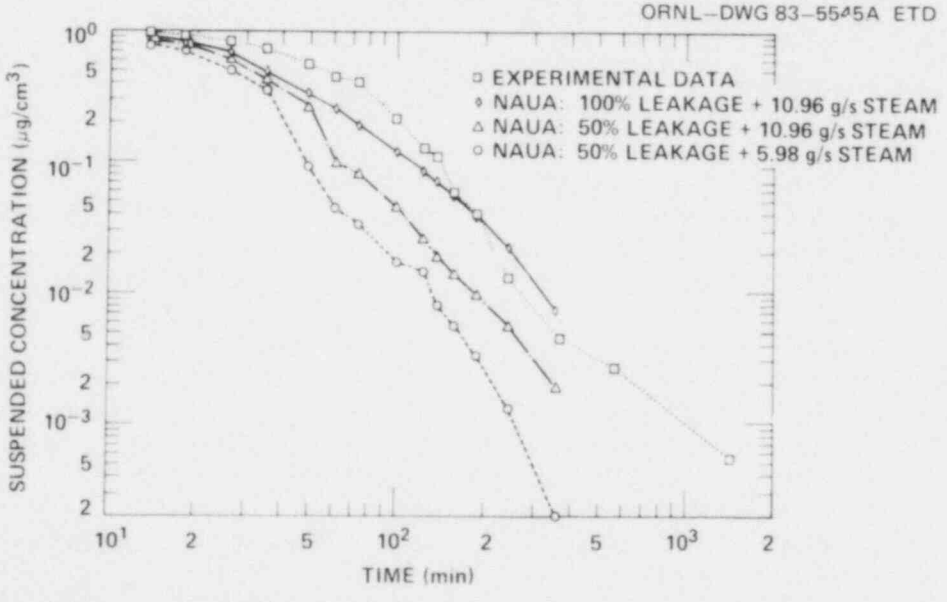

Fig. 32. Experiment 501, iron oxide in steam. Comparison of attempts to match experimental data using leakage to represent diffusiophoresis.

at the same steam injection rate raises the curve and changes its shape somewhat, but it is still too low. Finally, cutting both the leakage and the steam rates by one-half produces a smoothly declining curve, the highest of the three calculated curves, that does not resemble the experimental pattern too much even though the concentrations agree somewhat better. Figure 33 shows the results for the high-concentration experiment 504. Initially, the match is fairly good, but at long times, beyond about 150 min, the falloff in concentration is overestimated.

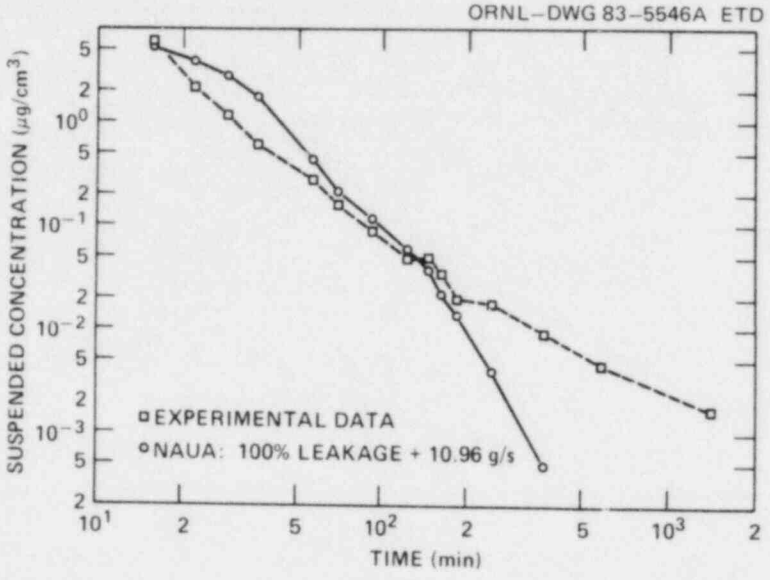

Fig. 33. Experiment 504, iron oxide in steam. Comparison of NAUA results using leakage to simulate diffusiophoresis.

3.2.5 Numerical effects

Finally, we note that a constant source of concern in a code of this kind is the effect that might be produced by the level of machine precision used and the number of size bins employed. Increases in both of these can greatly increase the cost and difficulty of running the program. It was found, however, that changing the machine precision did not greatly affect running time, nor were any serious quantitative effects noted. On the other hand, the use of additional size groups produced a more noticeable effect, as seen in Fig. 34, where increased channel number produced a somewhat greater disagreement with the experiment at earlier times. No qualitative aspects of the results appear affected, however. It appears safe, then, to use a low number of channels for surveys and to employ the more expensive 80+ channel calculations recommended by the code authors for final checks.

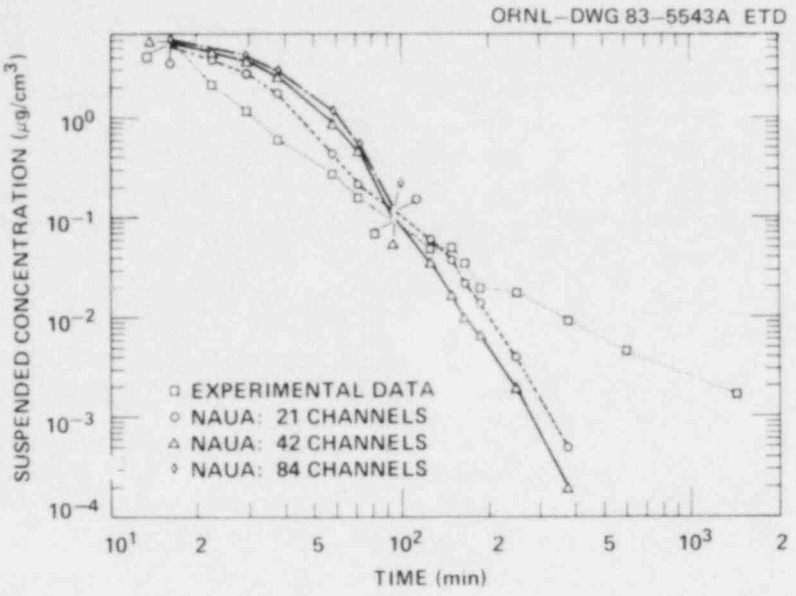

Fig. 34. Experiment 504. Tests of effect on results of using various number of size channels in NAUA.

3.2.6 Conclusions

These initial studies need to be examined more thoroughly. It is apparent that decisions concerning the proper input numbers for use in NAUA are not simple; it is not always clear, without examining the internal details of the code, just how the calculation is proceeding. This is particularly true with respect to the steam-source rate. The NSPP experiments are quite different in many respects from the KfK experiments that are used as a basis for the code. Further efforts will be needed to understand the code's limitations.

3.3 FAST-Related Code Development Work

J. C. Petrykowski

UVABUBL-II is a hybrid computer code being developed by Webb and Reynolds[15] at the University of Virginia to interpret data collected from the FAST experiments. The code utilizes features of UVABUBL[16] and SAMPAC[17] to model bubble dynamics in an axisymmetric geometry and can be readily adapted to the FAST pressure vessel geometry. The code currently contains models of

1. radiation heat transfer between bubble and coolant,
2. coolant mass transfer into bubble by surface vaporization and/or Rayleigh-Taylor surface instabilities,

3. fuel and coolant thermochemistry,
4. hydrodynamics of coolant and bubble using the Marker-and-Cell (MAC) method, and
5. real gas models of bubble and cover gas.

This code will provide a means for detailed investigations of the dynamics of high-temperature uranium-dioxide vapor bubbles under sodium for a wide range of conditions. Because many of the dynamics cannot be measured experimentally, the code is a necessary adjunct to the test program. If closure is obtained between the models contained in UVABUBL-II and the FAST experimental results, the code may be extended to analyze the bubble dynamics that could occur during a hypothetical hydrodynamic disassembly of an LMFBR core.

REFERENCES

1. R. E. Adams and M. L. Tobias, *Aerosol Release and Transport Program Quart. Prog. Rep. for July–September 1983*, NUREG/CR-3422, Vol. 3 (ORNL/TM-8849/V3), Union Carbide Corp. Nuclear Div., Oak Ridge Natl. Lab.

2. R. E. Adams and M. L. Tobias, *Aerosol Release and Transport Program Quart. Prog. Rep. for January–March 1982*, NUREG/CR-2809, Vol. 1 (ORNL/TM-8397/V1), Union Carbide Corp. Nuclear Div., Oak Ridge Natl. Lab.

3. R. E. Adams and M. L. Tobias, *Aerosol Release and Transport Program Quart. Prog. Rep. for October–December 1981*, NUREG/CR-2299, Vol. 4 (ORNL/TM-8307), Union Carbide Corp. Nuclear Div., Oak Ridge Natl. Lab.

4. R. E. Adams and M. L. Tobias, *Aerosol Release and Transport Program Quart. Prog. Rep. for April–June 1983*, NUREG/CR-3422, Vol. 2 (ORNL/TM-8849/V2), Union Carbide Corp. Nuclear Div., Oak Ridge Natl. Lab.

5. W. A. Zanotelli and G. D. Miller, *The Possible Mechanisms for the Formation of the Observed and Expected Compounds During a Hypothetical Core Disruptive Accident (HCDA)*, NUREG/CR-1134 (MLM-2637), Mound Facility, Miamisburg, Ohio, October 1979.

6. A. L. Wright et al., *Fuel Aerosol Simulant Test Data Record Report: Argon Tests*, NUREG/CR-1123 (ORNL/NUREG/TM-365), Union Carbide Corp. Nuclear Div., Oak Ridge Natl. Lab., March 1980.

7. A. B. Reynolds, J. L. Kelly, and M. E. McGowan, *Fission Product Release Model in CONACS*, UVA/532431/NEEP84/101, University of Virginia, October 1983.

8. G. W. Parker, G. E. Creek, and A. L. Sutton, Jr., "Core-Melt Aerosol Release and Transport," in *Aerosol Release and Transport Program Quart. Prog. Rep. for October–December 1982*, ed. R. E. Adams and M. L. Tobias, NUREG/CR-2809, Vol. 4 (ORNL/TM-8397/V4), Union Carbide Corp. Nuclear Div., Oak Ridge Natl. Lab.

9. H. Bunz, M. Koyro, and W. Schöck, "NAUA Mod 4. A Code for Calculating Aerosol Behavior in LWR Core Melt Accidents. Code Description and Users' Manual," presented at an EPRI workshop, Palo Alto, Calif., March 29–30, 1982; to be published as KfK-3554.

10. T. S. Kress and M. L. Tobias, *LMFBR Aerosol Release and Transport Quart. Prog. Rep. for January–March 1981*, NUREG/CR-2299, Vol. 1 (ORNL/TM-7946), Union Carbide Corp. Nuclear Div., Oak Ridge Natl. Lab.

11. T. S. Kress and M. L. Tobias, *LMFBR Aerosol Release and Transport Quart. Prog. Rep. for April–June 1981*, NUREG/CR-2299, Vol. 2 (ORNL/TM-7974), Union Carbide Corp. Nuclear Div., Oak Ridge Natl. Lab.

12. T. S. Kress and M. L. Tobias, *LMFBR Aerosol Release and Transport Quart. Prog. Rep. for July–September 1981*, NUREG/CR-2299, Vol. 3 (ORNL/TM-8149), Union Carbide Corp. Nuclear Div., Oak Ridge Natl. Lab.

13. R. E. Adams and M. L. Tobias, *Aerosol Release and Transport Program Quart. Prog. Rep. for April–June 1982*, NUREG/CR-2809, Vol. 2 (ORNL/TM-8397/V2), Union Carbide Corp. Nuclear Div., Oak Ridge Natl. Lab.

14. J. A. Gieseke, W. Lee, and L. D. Reed, *HAARM-3 Users Manual*, BMI-NUREG/1991, Battelle Memorial Institute, January 1978.

15. R. L. Webb and A. B. Reynolds, "Use of 2-Dimensional SAMPAC Code for Constraint for Analysis of FAST Experiments in Bubble Behavior and Aerosol Conditions" in *LMFBR Core Disruptive Accidents Annual Report, October 1981–September 1982*, UVA/532345/NEEP83/101, University of Virginia.

16. D. R. Bradley, "Heat, Mass, and Momentum Transfer from Large Two-Phase Bubbles," Ph.D. dissertation, The University of Virginia, Charlottesville, 1981.

17. S. S. Wang and J. H. Stuhmiller, "Analysis of Steam Chugging Phenomena," in *Vol. 3: SAMPAC Hydrodynamic Pool Response Code*, EPRI Fuel Report, Electric Power Research Institute, Palo Alto, Calif., 1979.

NUREG/CR-3830
Volume 1
ORNL/TM-9217/V1
Dist. Category R7

Internal Distribution

1-4. R. E. Adams
5. W. A. Bird
6. J. R. Buchanan
7. G. E. Creek (Consultant)
8. U. Gat
9. D. S. Griffith
10. C. V. Hardin
11. H. W. Hoffman
12. M. T. Hurst
13. A. L. Johnson
14. T. S. Kress
15. A. W. Longest
16. R. A. Lorenz
17. R. E. MacPherson
18. A. P. Malinauskas
19. G. W. Parker
20. J. C. Petrykowski
21. J. M. Rochelle
22. R. D. Spence
23. A. L. Sutton, Jr.
24. M. L. Tobias
25. H. E. Trammell
26. J. L. Wantland
27. R. P. Wichner
28. G. D. Whitman
29. A. L. Wright
30. ORNL Patent Office
31. Central Research Library
32. Document Reference Section
33-34. Laboratory Records Department
35. Laboratory Records (RC)

External Distribution

36. R. K. Hilliard, Westinghouse Hanford, P.O. Box 1970, Richland, WA 99352
37. R. Curtis, Division of Accident Evaluation, Nuclear Regulatory Commission, Washington, DC 20555
38. R. Hobbins, EG&G Idaho, P.O. Box 1625, Idaho Falls, ID 83415
39. Hans Jordan, Battelle Columbus Laboratories, 505 King Ave., Columbus, OH 43201
40. J. Larkins, Division of Accident Evaluation, Nuclear Regulatory Commission, Washington, DC 20555
41. R. L. Ritzman, Science Applications, Inc., 5 Palo Alto Square, Suite 2001, Palo Alto, CA 94304
42. M. Silberberg, Division of Accident Evaluation, Nuclear Regulatory Commission, Washington, DC 20555
43. J. Telford, Division of Accident Evaluation, Nuclear Regulatory Commission, Washington, DC 20555
44. T. Walker, Division of Accident Evaluation, Nuclear Regulatory Commission, Washington, DC 20555
45-49. Director, Office of Nuclear Regulatory Research, Nuclear Regulatory Commission, Washington, DC 20555
50. Office of Assistant Manager for Energy Research and Development, DOE, Oak Ridge Operations Office, Oak Ridge, TN 37831
51-52. Technical Information Center, DOE, Oak Ridge, TN 37831
53-302. Given distribution as shown in category R7 (NTIS-10)

NRC FORM 335 (11-81)

U.S. NUCLEAR REGULATORY COMMISSION

BIBLIOGRAPHIC DATA SHEET

1. REPORT NUMBER *(Assigned by DDC)*
NUREG/CR-3830/V1
ORNL/TM-9217/V1

4. TITLE AND SUBTITLE *(Add Volume No., if appropriate)*
Aerosol Release and Transport Semi-Annual Progress Report for October 1983–March 1984

2. *(Leave blank)*

3. RECIPIENT'S ACCESSION NO.

7. AUTHOR(S)
R. E. Adams, M. L. Tobias

5. DATE REPORT COMPLETED
MONTH: June | YEAR: 1984

9. PERFORMING ORGANIZATION NAME AND MAILING ADDRESS *(Include Zip Code)*
Oak Ridge National Laboratory
P. O. Box Y
Oak Ridge, TN 37831

DATE REPORT ISSUED
MONTH: July | YEAR: 1984

6. *(Leave blank)*

8. *(Leave blank)*

12. SPONSORING ORGANIZATION NAME AND MAILING ADDRESS *(Include Zip Code)*
Division of Accident Evaluation
Office of Nuclear Regulatory Research
U.S. Nuclear Regulatory Commission
Washington, D.C. 20555

10. PROJECT/TASK/WORK UNIT NO.

11. FIN NO.
B0121, B0476

13. TYPE OF REPORT
Semi-annual

PERIOD COVERED *(Inclusive dates)*
October 1983–March 1984

15. SUPPLEMENTARY NOTES

14. *(Leave blank)*

16. ABSTRACT *(200 words or less)*

This report summarizes progress for the Aerosol Release and Transport Program sponsored by the Nuclear Regulatory Commission, Office of Nuclear Regulatory Research, Division of Accident Evaluation, for the period October 1983–March 1984. Topics discussed include (1) the experimental program in the Fuel Aerosol Simulant Test (FAST) facility, (2) NSPP experiments involving mixtures of aerosols of iron oxide and uranium oxide in steam and dry atmospheres, (3) support work for the DEMONA (West Germany) and Marviken (Sweden) projects, (4) analysis of core melt experiments involving boric oxide volatility, (5) initial operation of the new 250-kW induction generator, (6) comparisons of NAUA results with experiments, and (7) tests and improvements in the UVABUBL-II code.

17. KEY WORDS AND DOCUMENT ANALYSIS

17a. DESCRIPTORS

17b. IDENTIFIERS/OPEN-ENDED TERMS

18. AVAILABILITY STATEMENT

19. SECURITY CLASS *(This report)*
UNCLASSIFIED

21. NO. OF PAGES

20. SECURITY CLASS *(This page)*
UNCLASSIFIED

22. PRICE
$

NRC FORM 335 (11-81)